bioRxiv preprint doi: https://doi.org/10.1101/2021.04.14.439704; this version posted April 14, 2021. The copyright holder for this preprint (which was not certified by peer review) is the author/funder. All rights reserved. No reuse allowed without permission.

Transcriptional Control of Brain Tumour Stem Cell Fate by a Carbohydrate Binding Protein

Ahmad Sharanek[1,2], Audrey Burban[1,2], Aldo Hernandez-Corchado[3,4], Idris Fatakdawala[1], Ariel Madrigal[3,4], Hamed S Najafabadi[3,4], Vahab D Soleimani[1,3], Arezu Jahani-Asl[1,2,5]

[1] Lady Davis Institute for Medical Research, Jewish General Hospital, Chemin de la Côte-Sainte-Catherine, Montréal, QC H3T 1E2, Canada

[2] Gerald Bronfman Department of Oncology and Division of Experimental Medicine, McGill University, Montréal, QC, Canada

[3] Department of Human Genetics, McGill University, 3640 Rue University Montréal, QC, H3A OC7, Canada

[4] McGill Genome Centre, 740 Dr. Penfield Avenue, Montreal, QC, H3A 0G1, Canada

[5] Integrated program in Neuroscience, Montréal Neurological Institute, 3801 University Street, Montréal, QC, H3A 2B4, Canada

To whom correspondence should be addressed:
Email: arezu.jahani@mcgill.ca
Tel: +1 514 340 8222 Ext 28438
Fax: +1 514 340 7502

bioRxiv preprint doi: https://doi.org/10.1101/2021.04.14.439704; this version posted April 14, 2021. The copyright holder for this preprint (which was not certified by peer review) is the author/funder. All rights reserved. No reuse allowed without permission.

Abstract

Brain tumour stem cells (BTSC) and intratumoural heterogeneity represent major challenges for the effective treatment of glioblastoma. EGFRvIII is a key oncogenic protein in glioblastoma, however, the mechanisms that regulate BTSC fate in EGFRvIII subtype of tumours remain poorly characterized. Here, we report our discovery of the lectin, galactoside-binding, soluble 1 (*LGALS1)* gene, encoding the carbohydrate binding protein, galectin1, as a key regulator of BTSC fate in glioblastoma tumours harbouring the EGFRvIII mutation. Genetic deletion of *LGALS1* alters gene expression profile of BTSCs, leads to cell cycle defects and impairs self-renewal. Using a combination of pharmacological and genetic approaches in preclinical animal models, we establish that inhibition of *LGALS1* signalling in BTSCs suppresses tumourigenesis, prolongs lifespan, and improves glioblastoma response to radiation-therapy. Mechanistically, two key transcription factors are involved in the regulation of *LGALS1* expression and function. Upstream, STAT3 directly binds to the promoter of *LGALS1* and robustly upregulates its expression. Downstream, galectin1 forms a complex with the transcription factor homeobox5 (HOXA5) to reprogram BTSC transcriptional landscape and drive glioblastoma tumourigenesis. Our data unravel a novel *LGALS1*/HOXA5 oncogenic signalling pathway that is required for BTSC maintenance and the pathogenesis of EGFRvIII subtype of glioblastoma.

bioRxiv preprint doi: https://doi.org/10.1101/2021.04.14.439704; this version posted April 14, 2021. The copyright holder for this preprint (which was not certified by peer review) is the author/funder. All rights reserved. No reuse allowed without permission.

Introduction

Glioblastoma is the most common and aggressive primary tumour in the adult brain. The current standard of care for glioblastoma patients includes surgical excision of the tumour followed by ionizing radiation (IR) and chemotherapy[1,2]. Despite these intense treatments, the median survival rate for glioblastoma patients remains 16-18 months[2,3]. Genetic and phenotypic heterogeneity in glioblastoma represent major challenges in glioblastoma therapy.

The Cancer Atlas Genome (TCGA) project has revealed that the receptor tyrosine kinases (RTK) are altered in 88% of the glioblastoma patients[4]. Epidermal growth factor receptor (EGFR) gene amplification occurs in approximately 40% of glioblastoma[5,6]. In addition, 63% to 75% of the glioblastoma that over-express EGFR are also found to have rearrangements of the EGFR gene, resulting in tumours expressing both wild-type EGFR and mutated EGFR[7-9]. The epidermal growth factor receptor variant III (EGFRvIII) is the most common EGFR activating mutation[10]. EGFRvIII leads to the induction of multiple oncogenic pathways including the activation of the transcription factor STAT3[11]. Despite the importance of EGFRvIII as a therapeutic target in glioblastoma, anti-EGFRvIII therapies including specific antibodies and tyrosine kinase inhibitors have not yet led to significant clinical therapy[12,13]. Identification of EGFRvIII dependent pathway(s) and drug targets to manipulate EGFRvIII in combination with complementary pathways represent promising therapeutic approaches.

Glioblastomas are cytogenetically heterogeneous tumours that frequently display chromosomal copy number alterations including the gain of whole chromosome 7. Recently, the gene encoding the transcription factor, Homeobox A5 (HOXA5), was reported to promote selection for the gain of chromosome 7 in human and mouse gliomas[14]. Importantly, the expression of HOXA5 correlated significantly with a more aggressive phenotype of glioblastoma[14]. The mechanisms that control HOXA5 function in glioblastoma remain largely unknown. Furthermore, the role of HOXA5 in EGFRvIII subtype of tumour is uncharacterized.

The lactose binding lectin, galectin1, encoded by the *LGALS1* gene, is a member of the carbohydrate binding proteins that are defined by their ability to recognize beta-galactose molecules found on cell surfaces and extracellular matrices[15]. Recent studies have found that

bioRxiv preprint doi: https://doi.org/10.1101/2021.04.14.439704; this version posted April 14, 2021. The copyright holder for this preprint (which was not certified by peer review) is the author/funder. All rights reserved. No reuse allowed without permission.

galectin1 is highly expressed in different human cancers including colon, breast, lung, head and neck, ovarian, prostate, and gliomas[16]. The upregulated expression of *LGALS1* in high-grade glioma correlates significantly with poor patient prognosis[17]. Higher extracellular galectin1 levels have been also detected in the plasma of glioblastoma patients[18]. Several findings highlight that galectin1 regulates glioblastoma tumour microenvironment and promotes migration[19], invasion[20], angiogenesis[21], and immune escape[22]. However, the role of *LGALS1* in cancer stem cells and in the genetic background of EGFRvIII, has remained unexplored.

Brain tumour stem cells (BTSCs) contribute to glioblastoma tumour heterogeneity by transitioning between different cell cycle states to: a) self-renew and sustain themselves, b) undergo persistent proliferation to contribute to tumour growth, c) differentiate and give rise to diverse cell populations to recapitulate the functional heterogeneity of the tumour, d) exit cell cycle and evade therapy, and e) re-enter cell cycle, and give rise to tumour recurrence[1,23-28]. Although these changes can stem from genetic alterations or response to environmental cues, the mechanisms that dictate BTSC fate are not fully understood. Defining the molecular mechanisms that govern BTSC fate in different glioblastoma subtypes is, therefore, critical for developing better treatments.

In the present study, we report a novel *LGALS1*/HOXA5 signalling pathway required for the pathogenesis of EGFRvIII-subtype of glioblastoma. Importantly, *LGALS1* confers resistance of glioblastoma tumours to ionizing radiation therapy via altering BTSC fate.

bioRxiv preprint doi: https://doi.org/10.1101/2021.04.14.439704; this version posted April 14, 2021. The copyright holder for this preprint (which was not certified by peer review) is the author/funder. All rights reserved. No reuse allowed without permission.

Results

Analysis of EGFRvIII candidate target genes in patient-derived BTSCs

To gain insights into EGFRvIII-gene signatures in patient-derived BTSCs, we analyzed public database in which RNA-Seq analysis of human BTSCs that naturally harbour EGFRvIII mutation or lack the mutation, were employed to establish EGFRvIII candidate target genes[29]. *LGALS1* scored among the top candidate target genes with its mRNA significantly upregulated in multiple EGFRvIII-expressing BTSC lines, raising the question of whether *LGALS1* plays a role in the regulation of BTSCs that harbour EGFRvIII mutation. To begin with, we subjected patient-derived BTSCs to immunoblotting analysis and confirmed that the expression levels of galectin1 protein were significantly upregulated in human BTSCs harbouring the EGFRvIII mutation compared to control BTSCs lacking the mutation (**Fig. 1a, Supplementary Fig. 1a**). Next, to establish whether *LGALS1* is a downstream target of EGFRvIII, we induced knockdown (KD) of *EGFRvIII/EGFR* using a pool of siRNAs in EGFRvIII-expressing BTSCs and subjected the cell lysates to RT-qPCR (**Supplementary Fig. 1b**) and immunoblotting analyses (**Fig. 1b-c**). Our data showed significant downregulation of *LGALS1* mRNA and galectin1 protein in *EGFRvIII* KD BTSCs (**Fig. 1 b-c and Supplementary Fig. 1b**). In parallel, we treated EGFRvIII-expressing BTSCs with lapatinib, an inhibitor of EGFR/EGFRvIII phosphorylation. Consistent with the results obtained following genetic KD of *EGFRvIII*, pharmacological inhibition of EGFRvIII by lapatinib significantly reduced galectin1 protein expression level as revealed by immunoblotting and immunostaining in multiple patient-derived BTSCs (**Fig. 1d-g**). Taken together, via analysis of patient-derived BTSC, as well as genetic and pharmacological approaches, we established that *LGALS1* is upregulated in an EGFRvIII-dependent manner in patient-derived BTSCs.

STAT3 directly binds the promoter of *LGALS1* to upregulate its expression

EGFRvIII and activated EGFR form a complex with the transcription factor STAT3 to direct signalling networks that drive tumourigenesis in different human cancers including glioblastoma[11,30-32]. For example, STAT3 directly occupies the promoters of *OSMR* and *iNOS,* two key regulators of oncogenesis, in EGFRvIII-expressing BTSCs and astrocytes to upregulate gene expression[29,33]. Analysis of the human *LGALS1* promoter revealed the presence of multiple STAT3 consensus motifs[34,35] (**Fig. 1h**). Strikingly, in analysis of patient-

bioRxiv preprint doi: https://doi.org/10.1101/2021.04.14.439704; this version posted April 14, 2021. The copyright holder for this preprint (which was not certified by peer review) is the author/funder. All rights reserved. No reuse allowed without permission.

derived BTSCs, we observed a positive correlation between galectin1 and phospho-STAT3 (Tyr705) protein expression levels (**Fig. 1i and Supplementary Fig 2a**), suggesting that *LGALS1* expression correlates with the activation of STAT3. We, thus, asked if EGFRvIII-mediated upregulation of *LGALS1* is controlled by STAT3. *LGALS1* expression levels were analyzed following pharmacological inhibition of STAT3 by WP1066 and S3I-201 or genetic KD of *STAT3* in two EGFRvIII-expressing BTSC73 and 147 (**Fig. 1j-o and Supplementary Fig. 2b-c**). We observed a significant decrease in *LGALS1* mRNA and galectin1 protein levels in *STAT3* KD BTSCs and BTSCs treated with either WP1066 or S3I-201 (**Fig. 1j-o and Supplementary Fig. 2b-c**). To determine whether endogenous STAT3 directly occupies the promoter of the *LGALS1* gene in EGFRvIII-expressing BTSCs, we performed ChIP-PCR and luciferase reporter assays in EGFRvIII-expressing BTSCs. In ChIP-PCR analysis, we subjected three different human BTSC lines (#73, 112, and 172), to immunoprecipitation (IP) using an endogenous STAT3 antibody or an IgG control. Our analysis revealed a significant enrichment of endogenous STAT3 at the endogenous *LGALS1* promoter across all the BTSCs (**Fig. 1p-r**). In analysis of the activity of the *LGALS1* promoter in transient expression assays, we found that the expression of a luciferase reporter gene that is controlled by 376 nt of the 5′ regulatory sequences of the *LGALS1* gene, was significantly downregulated upon deletion of STAT3 in mouse astrocytes (**Supplementary Fig. 2d**). Consistent with these results, we found that KD of *STAT3* gene by siRNA or pharmacological inhibition of STAT3 by WP1066 and S3I-201 in BTSC73 significantly attenuated the expression of the *LGALS1*-luciferase reporter gene (**Fig. 1s-t**). Taken together, we established that STAT3 directly occupies the promoter of *LGALS1* gene to upregulate its expression in EGFRvIII-expressing BTSCs.

***LGALS1* promotes the growth of EGFRvIII-expressing BTSCs**

EGFRvIII/STAT3 signalling plays crucial roles in cell growth and proliferation[36,37]. Identification of *LGALS1* as a direct downstream target gene of EGFRvIII/STAT3 oncogenic pathway in human BTSCs led us next to examine the role of *LGALS1* in the regulation of BTSC growth. We employed genetic approaches in which we induced KO or KD of *LGALS1* in EGFRvIII-expressing BTSCs using CRISPR-Cas9 or lentiviral-mediated transduction of BTSCs with shRNAs targeted against *LGALS1* mRNA, respectively (**Supplementary. Fig. 3 a-e**). We assessed cell viability by CellTiter-Glo luminescent cell viability assay in *LGALS1* CRISPR

bioRxiv preprint doi: https://doi.org/10.1101/2021.04.14.439704; this version posted April 14, 2021. The copyright holder for this preprint (which was not certified by peer review) is the author/funder. All rights reserved. No reuse allowed without permission.

EGFRvIII-expressing BTSC lines (#73 and 147) and found a marked reduction in cell viability in *LGALS1* CRISPR BTSCs compared to the corresponding control (**Fig. 2a-b**). Consistent with the results of cell viability assay, cell population growth assay showed that deletion of *LGALS1* resulted in a significant suppression of BTSC population growth (**Fig. 2c**). In other studies, we confirmed that KD of *LGALS1* using lentiviral transduction of two different shRNAs, also resulted in significant reduction of BTSC population growth (**Supplementary Fig. 3f**). Interestingly, the decrease of cell viability upon deletion of *LGALS1* was not associated with an induction of cell death as analyzed by flow cytometry for annexin V and propidium iodide (PI) (**Supplementary Fig. 3g-h**). We next assessed the impact of OTX008, the pharmacological inhibitor of galectin1. OTX008 is a small molecule calixarene derivative which is designed to bind specifically to the galectin1 amphipathic β-sheets leading to its oxidation and proteasomal degradation[38,39]. Treatment of BTSC73 and BTSC147 with OTX008 resulted in a dose-dependent inhibition of BTSC viability and growth (**Fig. 2d-f**). We confirmed that these differences were not due to toxicity or induction of apoptosis since 1-10 µM of OTX008 did not induce cell death as analyzed by annexin V/PI flow cytometry assay (**Supplementary Fig. 3i**). Furthermore, to establish the role of *LGALS1* in BTSC proliferation, we performed 5-ethynyl-2'-deoxyuridine (EdU) assay. We observed a drastic reduction in the number of EdU-incorporating BTSCs in *LGALS1* CRISPR (**Fig. 2g-i**) and OTX008-treated BTSC73 (**Supplementary Fig. 3j**). Our results demonstrate that *LGALS1* promotes growth and proliferation in EGFRvIII-expressing BTSCs.

Genetic knockdown of *LGALS1* or pharmacological inhibition of galectin1 impairs tumourigenic capacity of EGFRvIII-expressing BTSCs

EGFRvIII/STAT3 plays a key role in promoting glioblastoma tumourigenesis[11,40]. Our *in vitro* data in which *LGALS1* impaired the growth and proliferation of EGFRvIII-expressing BTSCs together with our discovery that *LGALS1* is a direct target of EGFRvIII/STAT3 signalling, raised the question of whether *LGALS1* regulates BTSC fate *in vivo* and promotes the growth of BTSC-derived tumours. To begin with, we subcutaneously injected *LGALS1* CRISPR or control EGFRvIII-expressing BTSC73 into the flank of 8-week-old immunodeficient (SCID) mice and assessed the ability of these cells to form tumours *in vivo*. Live imaging of luciferase activity was assessed using the *In Vivo* Imaging System (IVIS) allowing to trace tumour volume and confirm

bioRxiv preprint doi: https://doi.org/10.1101/2021.04.14.439704; this version posted April 14, 2021. The copyright holder for this preprint (which was not certified by peer review) is the author/funder. All rights reserved. No reuse allowed without permission.

that the tumours originated from the injected luciferase-expressing BTSCs (**Fig. 3a**). 3 weeks following injection, all mice in the control group harboured ulcerated tumours at the site of injection and had lost more than 20% of their body weight at end point. Strikingly, no tumours were formed in mice group receiving the *LGALS1* CRISPR BTSCs (**Fig. 3a-b**). Our data established that deletion of *LGALS1* impairs BTSC growth *in vivo*. Next, we assessed the impact of the pharmacological inhibition of galectin1 by OTX008 on tumour growth. We found that treatment of patient-derived xenografts with OTX008 significantly suppressed tumourigenesis in subcutaneous tumour assays performed with two different patient-derived BTSCs, BTSC73 (**Fig. 3c-d**) or BTSC147 (**Fig. 3e-f**).

To further investigate the impact of *LGALS1* deletion on brain tumour formation, we performed intracranial xenografts of *LGALS1* CRISPR or control EGFRvIII-expressing BTSC73 in immunodeficient SCID mice. Tumour volume was monitored via luciferase-based IVIS imaging (**Fig. 3g-h**). At 21 days following surgery, mice receiving control BTSC73 formed brain tumours and were at endpoint as assessed by major weight loss and neurological signs (**Fig. 3i**). Strikingly no tumours were found in any of the animals receiving *LGALS1* CRISPR BTSC73. To investigate the impact of *LGALS1* deletion on the animal lifespan, we maintained the animals for up to one year and assessed survival. Kaplan-Meier (KM) survival plots revealed that deletion of *LGALS1* in BTSC73 expanded the lifespan of the animals by ~9 months compared to only 21 days of mice bearing control BTSCs (**Fig. 3j**). Our data established that *LGALS1* is a key regulator of tumourigenesis in brain tumours harbouring EGFRvIII mutation.

Establishing *LGALS1* gene signatures in human BTSCs

Upstream of *LGALS1*, EGFRvIII/STAT3 signalling pathway functions to control the expression of *LGALS1* (**Fig. 1, Supplementary Fig. 1-2**). To dissociate downstream signalling pathways controlled by *LGALS1*, we subjected the *LGALS1* CRISPR and control EGFRvIII-expressing BTSC73, to mRNA-seq analyses (**Supplementary Fig. 4**). Gene-expression profiling revealed differentially expressed genes in *LGALS1* CRISPR BTSCs compared to control BTSC73, (adjusted p-value < 0.1) (**Fig. 4a**). We conducted GSEA enrichment analysis and found a significant downregulation of candidate target genes that are involved in the regulation of the cell cycle, including G2/M transition and mitotic spindle assembly (**Fig. 4b-c**). We validated the

bioRxiv preprint doi: https://doi.org/10.1101/2021.04.14.439704; this version posted April 14, 2021. The copyright holder for this preprint (which was not certified by peer review) is the author/funder. All rights reserved. No reuse allowed without permission.

changes in the mRNA expression of select cell cycle candidate target genes in two *LGALS1* CRISPR BTSCs (#73 and 147) by RT-qPCR analysis (**Fig. 4d-e**). Next, we examined the relevance of these transcriptional changes on the cell cycle regulation via performing cell cycle profiling by FACS analysis. Our data suggest that loss of *LGALS1* leads to an inhibition of cell cycle progression characterized by an accumulation of cells in the G2/M phase in multiple patient-derived EGFRvIII-expressing BTSCs (**Fig. 4f-i**), highlighting a role for *LGALS1* as a positive regulator of the cell cycle in EGFRvIII-expressing BTSCs.

LGALS1 regulates the self-renewal of EGFRvIII-expressing BTSCs

Cancer stem cells hijack transcriptional and epigenetic programs that endow them with a unique feature of long-term self-renewal potential, resulting in the continuous expansion of self-renewing cancer cells and tumour formation[41,42]. Cell cycle control is crucial for maintenance of stem cells self-renewal, and disruption of cell cycle regulators has been shown to impair stem cell self-renewal[43], raising the question of whether *LGALS1* promotes BTSC self-renewal capacity. To examine the impact of *LGALS1* on self-renewal, we subjected *LGALS1* CRISPR and control EGFRvIII-expressing BTSCs to limiting dilution assay (LDA) and extreme limiting dilution assay (ELDA)[44]. Strikingly, deletion of *LGALS1* resulted in a significant decrease in sphere numbers and sphere-formation frequency compared to corresponding controls (**Fig. 5a-d, Supplementary Fig. 5a**). Consistent with this data, KD of *LGALS1* by lentiviral transduction of two different shRNAs (**Supplementary Fig 5b-c**) or transient KD of *LGALS1* using *a* pool of siRNAs (**Supplementary Fig. 5d-e**), significantly decreased BTSC self-renewal. Given that *LGALS1* is upregulated in an EGFRvIII-dependent manner, we sought to examine whether *LGALS1*-mediated regulation of BTSC self-renewal is specific to EGFRvIII cohort of BTSCs. We, therefore, induced the KD of *LGALS1* in two patient-derived BTSCs that do not harbour EGFRvIII mutation (#12, 30) and subjected the cells to LDA and ELDA analyses. Our results demonstrated that KD of *LGALS1* had no significant impact on the number of spheres (**Fig. 5e-f**) or the frequency of sphere-formation (**Fig. 5g-h**), perhaps due to low expression levels of *LGALS1* in BTSCs lacking the EGFRvIII mutation.

In another set of independent experiments, we sought to examine how EGFRvIII-expressing BTSCs or BTSCs lacking the mutation respond to the pharmacological inhibitor, OTX008.

bioRxiv preprint doi: https://doi.org/10.1101/2021.04.14.439704; this version posted April 14, 2021. The copyright holder for this preprint (which was not certified by peer review) is the author/funder. All rights reserved. No reuse allowed without permission.

EGFRvIII-expressing BTSC lines (#73, 147, 68, 112, and 172) and BTSC control lines that do not harbour EGFRvIII mutation (#12 and 30) were subjected to LDA and ELDA, following treatment with different concentrations of OTX008 or a vehicle control. Our analysis revealed that OTX008 resulted in a significant decrease in the number of spheres and self-renewal capacity in all the EGFRvIII-expressing BTSCs examined (**Fig. 5i-p and Supplementary Fig. 5f-g**). Importantly, we observed a dose-dependent effect in OTX008-mediated suppression of self-renewal. In contrast, OTX008 had no significant impact on the self-renewal of BTSCs that do not harbour EGFRvIII mutation (**Fig. 5q-t**). In summary, using genetic and pharmacological approaches, we establish a role of *LGALS1* in regulation of EGFRvIII-expressing BTSCs.

Pharmacological targeting of galectin1 sensitizes glioblastoma to IR and expands lifespan

Tumours that are highly resistant to ionizing radiation (IR) including glioma, melanoma, and prostate cancer are found to express high levels of galectin1[45], raising the question of whether galectin1 may contribute to BTSC resistance in response to IR. To address this question, we employed ELDA analysis to assess the response of *LGALS1* CRISPR and control BTSC73 to 4 Gy of IR. IR induced 2.7-fold decrease in stem cell frequency of control BTSC73 Strikingly, deletion of *LGALS1* sensitized the BTSC73 response to IR by 14 folds (**Fig. 6a-b**). Since exposure to IR provokes DNA damage that trigger cell death[46], we analyzed cell death by annexin V and PI double staining and we found that loss of *LGALS1* resulted in a significant increase in IR-induced apoptosis, whereby 53% of irradiated *LGALS1* CRISPR BTSCs were positive for annexin V compared to only 22% in the irradiated control BTSCs (**Fig. 6c-d**). These data suggest that *LGALS1* targeting sensitizes BTSCs to IR-induced cell death.

To investigate the functional relevance of these findings to glioblastoma *in vivo*, we transplanted EGFRvIII-expressing BTSC73 into the brains of immunodeficient mice and assessed whether combinational therapy with IR and pharmacological inhibition of galectin1 by OTX008 improves the lifespan of the animals. Mice bearing BTSCs were treated with: vehicle control (PBS), OTX008 (10 mg/kg), IR (4 Gy) or the combination of OTX008 and IR (**Fig. 6e**). At 21 days following surgery, mice receiving control BTSC73 formed brain tumours and were at endpoint as assessed by major weight loss and neurological signs (**Fig. 6f-h**). Exposure to 4

bioRxiv preprint doi: https://doi.org/10.1101/2021.04.14.439704; this version posted April 14, 2021. The copyright holder for this preprint (which was not certified by peer review) is the author/funder. All rights reserved. No reuse allowed without permission.

Gy of IR or treatment with OTX008 delayed tumourigenesis, whereby mice exposed to IR or treated with OTX008 were at endpoint at 30 and 36 days, respectively (**Fig. 6f-h**). Strikingly, the combined OTX008 and IR significantly suppressed tumourigenesis and extended survival past 65 days (**Fig. 6f-j**). These data established the benefit of co-targeting the resistant EGFRvIII-expressing tumours with OTX008 and IR.

Galectin1 physically and functionally interacts with the transcription factor HOXA5

To address the mechanistic basis of how *LGALS1* may regulate BTSC fate, glioblastoma tumourigenesis, cell cycle, and resistance to IR, we applied additional analysis to *LGALS1* regulated genes established via RNA-seq analysis. First, *LGALS1*-differentially regulated genes (**Supplementary Fig. 4**) were subjected to enrichment analysis of transcription factor (TF) binding motifs using oPOSSUM-3 software to screen for TFs that could cooperate with galectin1 to reprogram transcriptional landscape. This analysis led to the identification of the over-represented TF binding sites in the promoter of *LGALS1*-differentially expressed genes. The five transcription factors HOXA5, Pdx1, SRY, Nkx2-5, and ARID3A binding sites were significantly enriched within the promoter regions (Z-Score > mean + 2sd) (**Fig. 7a**). After filtering of these 5 candidate TFs, HOXA5, a member of the homeobox TF family, was selected for further investigation based on the following criteria: **First**, HOXA5 ranked first whereby 70% of galectin1 potential target genes harbour the consensus motif for HOXA5 binding (**Fig. 7a-b**). **Second**, HOXA5 was recently suggested to promote an aggressive phenotype of glioblastoma associated with gain of chromosome 7[14]**. Third**, it has been shown that HOXA5 regulates cell cycle of glioblastoma cells and mediates their resistance to IR[14]. **Fourth**, the role of HOXA5 remains unexplored in EGFRvIII-subtype of glioblastoma.

To begin with, we sought to validate the enrichment of HOXA5 binding sites on the *LGALS1*-differentially regulated genes. Thus, we queried the public available ChIP-seq data of human carcinoma cells[47] and we analyzed the genomic distribution of HOXA5 ChIP-seq peaks relative to the *LGALS1*-differentially regulated genes in BTSCs. We found a significant abundance of HOXA5 ChIP-Seq peaks in the 5′ untranslated region and promoter of *LGALS1* candidate target genes (**Fig. 7c**), suggesting that *LGALS1*-differentially regulated genes are direct HOXA5 targets.

bioRxiv preprint doi: https://doi.org/10.1101/2021.04.14.439704; this version posted April 14, 2021. The copyright holder for this preprint (which was not certified by peer review) is the author/funder. All rights reserved. No reuse allowed without permission.

Prior to addressing whether galectin1 cooperates with HOXA5 to redirect transcription in BTSCs, we examined HOXA5 expression in EGFRvIII-expressing BTSCs. Interestingly, similar to galectin1, HOXA5 protein levels were significantly higher in the EGFRvIII-expressing BTSCs (**Fig. 7d**), and the Pearson correlation analysis revealed a strong correlation between galectin1, HOXA5 and EGFRvIII expression in BTSCs (**Fig. 7e**). Next, we induced the KD of *HOXA5* by a pool of siRNA followed by RT-q-PCR for select cell cycle related genes that are downregulated in *LGALS1* CRISPR and possess HOXA5 binding motifs. Strikingly, similar to the effect of *LGALS1* deletion, we found a significant reduction in the mRNA levels of the 10 randomly selected cell cycle related genes in two patient-derived EGFRvIII-expressing BTSCs (#73 and 147) (**Fig. 7f-g**). To further establish if loss of *HOXA5* phenocopies the *LGALS1*-KO phenotype, we examined the impact of *HOXA5* KD on the self-renewal of EGFRvIII-expressing BTSCs. ELDA analysis revealed that similar to *LGALS1* deletion, KD of *HOXA5* significantly reduced the stem cell frequency in BTSC73. Second, we examined whether *HOXA5* KD phenocopies *LGALS1* effects by conferring resistance of EGFRvIII-expressing BTSCs to IR. *HOXA5* KD and control EGFRvIII-expressing BTSCs were exposed to 4 Gy of IR, followed by ELDA analysis. Our data revealed a significant decrease in sphere formation frequency in irradiated *HOXA5* KD BTSCs compared to BTSC control (**Fig. 7h-i**). These results established that *HOXA5* KD in BTSCs phenocopies the effects of *LGALS1* deletion and suggest a cross-talk between galectin1 and HOXA5 in reprogramming the BTSC transcriptional network.

Our findings in which we established a functional interaction between galectin1 and HOXA5 in regulation of BTSC fate led us next to assess whether galectin1 physically interacts with HOXA5 in EGFRvIII-expressing BTSCs. We employed immunostaining and co-immunoprecipitation (co-IP) experiments to examine protein-protein interactions. Strikingly, we found that HOXA5 physically interacts with galectin1 endogenously in multiple patient-derived EGFRvIII-expressing BTSCs (**Fig. 7j-m**). To validate this interaction *in situ*, we performed proximity ligation assay (PLA). PLA can detect protein-protein interaction at single cell resolution[48]. We detected significant PLA signals in multiple EGFRvIII-expressing BTSCs in which antibodies to HOXA5 and galectin1 were employed (**Fig. 7n-q**). Importantly, deletion of *LGALS1* abolished the PLA interaction signal (**Fig. 7q**).

bioRxiv preprint doi: https://doi.org/10.1101/2021.04.14.439704; this version posted April 14, 2021. The copyright holder for this preprint (which was not certified by peer review) is the author/funder. All rights reserved. No reuse allowed without permission.

Since TFs function by binding to the gene regulatory regions to control expression, we next examined if the galectin1/HOXA5 interaction is required for HOXA5 DNA binding activity. We performed ChIP assay for HOXA5 in *LGALS1* CRISPR and CTL BTSC73, followed by qPCR for select *LGALS1*-downregulated genes that possess HOXA5 binding motifs. ChIP-PCR revealed an enrichment of HOXA5 on the promoter regions of the potential target genes in the BTSC73 CTL, however, silencing of *LGALS1* significantly impaired the binding of HOXA5 to the promoter of its target genes (**Fig. 7r**). Together, these data established that galectin1 forms a complex with the TF HOXA5 and this interaction is essential for HOXA5 TF activity to reprogram BTSC transcriptional programs.

Finally, having established that galectin1 mediates its effects through a cross-talk with HOXA5, we sought to determine the prognostic value of galectin1/HOXA5 expression in human glioblastoma patients in the response to IR. We employed the TCGA (microarray G4502A) in which IR treatment data and patient's response to therapy were available. We generated KM survival plots for glioblastoma patients after clustering them based on the mRNA expression levels of *LGALS1* and HOXA5 into high (above median) and low (below median). Our analyses demonstrated that patients with low expression of *LGALS1* and *HOXA5* had best prognosis in response to IR (**Fig. 7s-t**). Our data highlights the importance of galectin1/HOXA5 targeting in combination with IR as a potential promising therapeutic regimen for glioblastoma.

bioRxiv preprint doi: https://doi.org/10.1101/2021.04.14.439704; this version posted April 14, 2021. The copyright holder for this preprint (which was not certified by peer review) is the author/funder. All rights reserved. No reuse allowed without permission.

Discussion

In the present study, we report a novel role for the *LGALS1* gene, encoding the carbohydrate binding protein, galectin1, in maintaining the EGFRvIII/STAT3 oncogenic signalling in glioma stem cells and conferring glioblastoma resistance to therapy. Beginning with loss and gain of function studies using genetic and pharmacological approaches we found that *LGALS1* is upregulated in an EGFRvIII and STAT3 dependent manner. We employed ChIP and luciferase reporter assays and showed that STAT3 directly occupies the promoter of *LGALS1* in EGFRvIII-expressing BTSCs and upregulates its expression. Importantly, using genetic and pharmacological approaches we established that inhibition of this signalling pathway robustly impairs the self-renewal and growth of BTSCs and sensitizes the response of glioblastoma tumours to IR. Finally, via RNA-seq analysis followed by unbiased TF enrichment analysis, ChIP-seq analysis, proximity ligation assay and endogenous co-immunoprecipitation experiments, we established that galectin1 physically and functionally interacts with the homeobox TF, HOXA5, to reprogram BTSC transcriptional network and confer glioblastoma resistance to IR. Our data unravel a novel STAT3/*LGALS1*/HOXA5 signalling axis that tightly regulates the pathogenesis of EGFRvIII subtype of glioblastoma via altering BTSC fate.

Epigenomic and transcriptomic analyses have revealed that EGFRvIII specifically controls gene regulatory regions and impacts glioblastoma response to therapy via modulating transcription[49]. EGFRvIII forms a complex with STAT3 to control gene regulation and glioblastoma tumourigenesis[11,33]. Our findings that *LGALS1* is a direct transcriptional target of EGFRvIII/STAT3 and required for the pathogenesis of EGFRvIII subtype of glioblastoma, raises important implications for developing novel therapeutic regimen that includes a combination of EGFRvIII/STAT3 and galectin1 inhibitors. Furthermore, our findings that *LGALS1* is required to maintain BTSC pool specifically in EGFRvIII-expressing cancer stem cells, opens new avenues to assess its potential as a biomarker for the EGFRvIII subtype of glioblastoma.

In this study, we provide significant preclinical and mechanistic data to show that galectin1 cooperates with HOXA5 to reprogram BTSC gene signatures. As with most homeobox TFs, the regulatory mechanisms governing HOXA5 activity remain largely

bioRxiv preprint doi: https://doi.org/10.1101/2021.04.14.439704; this version posted April 14, 2021. The copyright holder for this preprint (which was not certified by peer review) is the author/funder. All rights reserved. No reuse allowed without permission.

unknown. Our data suggests that galectin1 is an important regulator of HOXA5 function and deletion of galectin1 significantly impairs HOXA5 TF activity. Whether galectin1 functions as a co-transcription factor in this context or facilitates the nuclear translocation of HOXA5 remain to be investigated in future studies.

HOXA5 has been previously shown as a positive regulator of TP53 in solid tumours such as breast and lung cancer[50]. Our study provides strong experimental evidence that in the genetic background of EGFRvIII, HOXA5 functions in an oncogenic capacity. Interestingly, STAT3 which functions as a tumour suppressor in PTEN deficient glioblastoma, promotes tumourigenesis in the genetic background of EGFRvIII[11]. Our finding that STAT3 and HOXA5 function on the same signalling pathway to direct galectin1 expression and function, provides further proof that HOXA5 function in an oncogenic capacity in EGFRvIII subtype of glioblastoma.

In conclusion, our data unravel a novel role for the carbohydrate binding protein, galectin1, in the pathogenesis of EGFRvIII mutant glioma stem cells and tumourigenesis via a cross talk with the transcription factor HOXA5. Our data highlights the importance of galectin1-HOXA5 targeting as a promising approach to deplete malignant cancer stem cells in the EGFRvIII subtype of glioblastoma.

bioRxiv preprint doi: https://doi.org/10.1101/2021.04.14.439704; this version posted April 14, 2021. The copyright holder for this preprint (which was not certified by peer review) is the author/funder. All rights reserved. No reuse allowed without permission.

References

1 Chen, J., McKay, R. M. & Parada, L. F. Malignant glioma: lessons from genomics, mouse models, and stem cells. *Cell* **149**, 36-47, doi:10.1016/j.cell.2012.03.009 (2012).

2 Stupp, R. *et al.* Radiotherapy plus concomitant and adjuvant temozolomide for glioblastoma. *N Engl J Med* **352**, 987-996, doi:10.1056/NEJMoa043330 (2005).

3 Chinot, O. L. *et al.* Bevacizumab plus radiotherapy-temozolomide for newly diagnosed glioblastoma. *The New England journal of medicine* **370**, 709-722, doi:10.1056/NEJMoa1308345 (2014).

4 Cancer Genome Atlas Research, N. Comprehensive genomic characterization defines human glioblastoma genes and core pathways. *Nature* **455**, 1061-1068, doi:10.1038/nature07385 (2008).

5 Wong, A. J. *et al.* Structural alterations of the epidermal growth factor receptor gene in human gliomas. *Proceedings of the National Academy of Sciences of the United States of America* **89**, 2965-2969, doi:10.1073/pnas.89.7.2965 (1992).

6 Furnari, F. B. *et al.* Malignant astrocytic glioma: genetics, biology, and paths to treatment. *Genes & development* **21**, 2683-2710, doi:10.1101/gad.1596707 (2007).

7 Ekstrand, A. J. *et al.* Genes for epidermal growth factor receptor, transforming growth factor alpha, and epidermal growth factor and their expression in human gliomas in vivo. *Cancer research* **51**, 2164-2172 (1991).

8 Ekstrand, A. J., Sugawa, N., James, C. D. & Collins, V. P. Amplified and rearranged epidermal growth factor receptor genes in human glioblastomas reveal deletions of sequences encoding portions of the N- and/or C-terminal tails. *Proceedings of the National Academy of Sciences of the United States of America* **89**, 4309-4313, doi:10.1073/pnas.89.10.4309 (1992).

9 Malden, L. T., Novak, U., Kaye, A. H. & Burgess, A. W. Selective amplification of the cytoplasmic domain of the epidermal growth factor receptor gene in glioblastoma multiforme. *Cancer research* **48**, 2711-2714 (1988).

10 Wikstrand, C. J. *et al.* Monoclonal antibodies against EGFRvIII are tumor specific and react with breast and lung carcinomas and malignant gliomas. *Cancer research* **55**, 3140-3148 (1995).

bioRxiv preprint doi: https://doi.org/10.1101/2021.04.14.439704; this version posted April 14, 2021. The copyright holder for this preprint (which was not certified by peer review) is the author/funder. All rights reserved. No reuse allowed without permission.

11 de la Iglesia, N. *et al.* Identification of a PTEN-regulated STAT3 brain tumor suppressor pathway. *Genes & development* **22**, 449-462, doi:10.1101/gad.1606508 (2008).

12 Raizer, J. J. *et al.* A phase II trial of erlotinib in patients with recurrent malignant gliomas and nonprogressive glioblastoma multiforme postradiation therapy. *Neuro-oncology* **12**, 95-103, doi:10.1093/neuonc/nop015 (2010).

13 Reardon, D. A. *et al.* Phase I/randomized phase II study of afatinib, an irreversible ErbB family blocker, with or without protracted temozolomide in adults with recurrent glioblastoma. *Neuro-oncology* **17**, 430-439, doi:10.1093/neuonc/nou160 (2015).

14 Cimino, P. J. *et al.* Increased HOXA5 expression provides a selective advantage for gain of whole chromosome 7 in IDH wild-type glioblastoma. *Genes Dev* **32**, 512-523, doi:10.1101/gad.312157.118 (2018).

15 Liu, F. T. & Rabinovich, G. A. Galectins as modulators of tumour progression. *Nature reviews. Cancer* **5**, 29-41, doi:10.1038/nrc1527 (2005).

16 Astorgues-Xerri, L. *et al.* Unraveling galectin-1 as a novel therapeutic target for cancer. *Cancer treatment reviews* **40**, 307-319, doi:10.1016/j.ctrv.2013.07.007 (2014).

17 Rorive, S. *et al.* Galectin-1 is highly expressed in human gliomas with relevance for modulation of invasion of tumor astrocytes into the brain parenchyma. *Glia* **33**, 241-255, doi:10.1002/1098-1136(200103)33:3<241::aid-glia1023>3.0.co;2-1 (2001).

18 Kros, J. M. *et al.* Circulating glioma biomarkers. *Neuro-oncology* **17**, 343-360, doi:10.1093/neuonc/nou207 (2015).

19 Camby, I., Le Mercier, M., Lefranc, F. & Kiss, R. Galectin-1: a small protein with major functions. *Glycobiology* **16**, 137R-157R, doi:10.1093/glycob/cwl025 (2006).

20 Toussaint, L. G., 3rd *et al.* Galectin-1, a gene preferentially expressed at the tumor margin, promotes glioblastoma cell invasion. *Molecular cancer* **11**, 32, doi:10.1186/1476-4598-11-32 (2012).

21 Le Mercier, M. *et al.* Knocking down galectin 1 in human hs683 glioblastoma cells impairs both angiogenesis and endoplasmic reticulum stress responses. *Journal of neuropathology and experimental neurology* **67**, 456-469, doi:10.1097/NEN.0b013e318170f892 (2008).

22 Verschuere, T. *et al.* Glioma-derived galectin-1 regulates innate and adaptive antitumor immunity. *International journal of cancer* **134**, 873-884, doi:10.1002/ijc.28426 (2014).

bioRxiv preprint doi: https://doi.org/10.1101/2021.04.14.439704; this version posted April 14, 2021. The copyright holder for this preprint (which was not certified by peer review) is the author/funder. All rights reserved. No reuse allowed without permission.

23 Singh, S. K. *et al.* Identification of human brain tumour initiating cells. *Nature* **432**, 396-401, doi:10.1038/nature03128 (2004).

24 Galli, R. *et al.* Isolation and characterization of tumorigenic, stem-like neural precursors from human glioblastoma. *Cancer Res* **64**, 7011-7021, doi:10.1158/0008-5472.CAN-04-1364 (2004).

25 Lathia, J. D., Mack, S. C., Mulkearns-Hubert, E. E., Valentim, C. L. & Rich, J. N. Cancer stem cells in glioblastoma. *Genes & development* **29**, 1203-1217, doi:10.1101/gad.261982.115 (2015).

26 Chen, J. *et al.* A restricted cell population propagates glioblastoma growth after chemotherapy. *Nature* **488**, 522-526, doi:10.1038/nature11287 (2012).

27 Bao, S. *et al.* Glioma stem cells promote radioresistance by preferential activation of the DNA damage response. *Nature* **444**, 756-760, doi:10.1038/nature05236 (2006).

28 Venugopal, C. *et al.* Pyrvinium Targets CD133 in Human Glioblastoma Brain Tumor-Initiating Cells. *Clin Cancer Res* **21**, 5324-5337, doi:10.1158/1078-0432.CCR-14-3147 (2015).

29 Jahani-Asl, A. *et al.* Control of glioblastoma tumorigenesis by feed-forward cytokine signaling. *Nature neuroscience* **19**, 798-806, doi:10.1038/nn.4295 (2016).

30 de la Iglesia, N., Puram, S. V. & Bonni, A. STAT3 regulation of glioblastoma pathogenesis. *Current molecular medicine* **9**, 580-590, doi:10.2174/156652409788488739 (2009).

31 Wheeler, S. E. *et al.* Epidermal growth factor receptor variant III mediates head and neck cancer cell invasion via STAT3 activation. *Oncogene* **29**, 5135-5145, doi:10.1038/onc.2009.279 (2010).

32 Lo, H. W. *et al.* Nuclear interaction of EGFR and STAT3 in the activation of the iNOS/NO pathway. *Cancer cell* **7**, 575-589, doi:10.1016/j.ccr.2005.05.007 (2005).

33 Puram, S. V. *et al.* STAT3-iNOS Signaling Mediates EGFRvIII-Induced Glial Proliferation and Transformation. *The Journal of neuroscience : the official journal of the Society for Neuroscience* **32**, 7806-7818, doi:10.1523/JNEUROSCI.3243-11.2012 (2012).

34 Seidel, H. M. *et al.* Spacing of palindromic half sites as a determinant of selective STAT (signal transducers and activators of transcription) DNA binding and transcriptional

bioRxiv preprint doi: https://doi.org/10.1101/2021.04.14.439704; this version posted April 14, 2021. The copyright holder for this preprint (which was not certified by peer review) is the author/funder. All rights reserved. No reuse allowed without permission.

activity. *Proceedings of the National Academy of Sciences of the United States of America* **92**, 3041-3045, doi:10.1073/pnas.92.7.3041 (1995).

35 Schaefer, T. S., Sanders, L. K. & Nathans, D. Cooperative transcriptional activity of Jun and Stat3 beta, a short form of Stat3. *Proceedings of the National Academy of Sciences of the United States of America* **92**, 9097-9101, doi:10.1073/pnas.92.20.9097 (1995).

36 Stechishin, O. D. *et al.* On-target JAK2/STAT3 inhibition slows disease progression in orthotopic xenografts of human glioblastoma brain tumor stem cells. *Neuro-oncology* **15**, 198-207, doi:10.1093/neuonc/nos302 (2013).

37 Jensen, K. V., Hao, X., Aman, A., Luchman, H. A. & Weiss, S. EGFR blockade in GBM brain tumor stem cells synergizes with JAK2/STAT3 pathway inhibition to abrogate compensatory mechanisms in vitro and in vivo. *Neuro-oncology advances* **2**, vdaa020, doi:10.1093/noajnl/vdaa020 (2020).

38 Astorgues-Xerri, L. *et al.* OTX008, a selective small-molecule inhibitor of galectin-1, downregulates cancer cell proliferation, invasion and tumour angiogenesis. *European journal of cancer* **50**, 2463-2477, doi:10.1016/j.ejca.2014.06.015 (2014).

39 Leung, Z. *et al.* Galectin-1 promotes hepatocellular carcinoma and the combined therapeutic effect of OTX008 galectin-1 inhibitor and sorafenib in tumor cells. *J Exp Clin Cancer Res* **38**, 423, doi:10.1186/s13046-019-1402-x (2019).

40 Fan, Q. W. *et al.* EGFR phosphorylates tumor-derived EGFRvIII driving STAT3/5 and progression in glioblastoma. *Cancer cell* **24**, 438-449, doi:10.1016/j.ccr.2013.09.004 (2013).

41 Brooks, M. D., Burness, M. L. & Wicha, M. S. Therapeutic Implications of Cellular Heterogeneity and Plasticity in Breast Cancer. *Cell stem cell* **17**, 260-271, doi:10.1016/j.stem.2015.08.014 (2015).

42 Kreso, A. & Dick, J. E. Evolution of the cancer stem cell model. *Cell stem cell* **14**, 275-291, doi:10.1016/j.stem.2014.02.006 (2014).

43 He, S., Nakada, D. & Morrison, S. J. Mechanisms of stem cell self-renewal. *Annual review of cell and developmental biology* **25**, 377-406, doi:10.1146/annurev.cellbio.042308.113248 (2009).

bioRxiv preprint doi: https://doi.org/10.1101/2021.04.14.439704; this version posted April 14, 2021. The copyright holder for this preprint (which was not certified by peer review) is the author/funder. All rights reserved. No reuse allowed without permission.

44 Hu, Y. & Smyth, G. K. ELDA: extreme limiting dilution analysis for comparing depleted and enriched populations in stem cell and other assays. *Journal of immunological methods* **347**, 70-78, doi:10.1016/j.jim.2009.06.008 (2009).

45 Navarro, P., Martinez-Bosch, N., Blidner, A. G. & Rabinovich, G. A. Impact of Galectins in Resistance to Anticancer Therapies. *Clinical cancer research : an official journal of the American Association for Cancer Research* **26**, 6086-6101, doi:10.1158/1078-0432.CCR-18-3870 (2020).

46 Afshar, G. *et al.* Radiation-induced caspase-8 mediates p53-independent apoptosis in glioma cells. *Cancer research* **66**, 4223-4232, doi:10.1158/0008-5472.CAN-05-1283 (2006).

47 Yan, J. *et al.* Transcription factor binding in human cells occurs in dense clusters formed around cohesin anchor sites. *Cell* **154**, 801-813, doi:10.1016/j.cell.2013.07.034 (2013).

48 Soderberg, O. *et al.* Direct observation of individual endogenous protein complexes in situ by proximity ligation. *Nature methods* **3**, 995-1000, doi:10.1038/nmeth947 (2006).

49 Liu, F. *et al.* EGFR Mutation Promotes Glioblastoma through Epigenome and Transcription Factor Network Remodeling. *Molecular cell* **60**, 307-318, doi:10.1016/j.molcel.2015.09.002 (2015).

50 Raman, V. *et al.* Compromised HOXA5 function can limit p53 expression in human breast tumours. *Nature* **405**, 974-978, doi:10.1038/35016125 (2000).

51 Love, M. I., Huber, W. & Anders, S. Moderated estimation of fold change and dispersion for RNA-seq data with DESeq2. *Genome biology* **15**, 550, doi:10.1186/s13059-014-0550-8 (2014).

52 Ignatiadis, N., Klaus, B., Zaugg, J. B. & Huber, W. Data-driven hypothesis weighting increases detection power in genome-scale multiple testing. *Nature methods* **13**, 577-580, doi:10.1038/nmeth.3885 (2016).

53 Soleimani, V. D., Palidwor, G. A., Ramachandran, P., Perkins, T. J. & Rudnicki, M. A. Chromatin tandem affinity purification sequencing. *Nature protocols* **8**, 1525-1534, doi:10.1038/nprot.2013.088 (2013).

54 Colaprico, A. *et al.* TCGAbiolinks: an R/Bioconductor package for integrative analysis of TCGA data. *Nucleic acids research* **44**, e71, doi:10.1093/nar/gkv1507 (2016).

bioRxiv preprint doi: https://doi.org/10.1101/2021.04.14.439704; this version posted April 14, 2021. The copyright holder for this preprint (which was not certified by peer review) is the author/funder. All rights reserved. No reuse allowed without permission.

55 Sharanek, A. *et al.* OSMR controls glioma stem cell respiration and confers resistance of glioblastoma to ionizing radiation. *Nature communications* **11**, 4116, doi:10.1038/s41467-020-17885-z (2020).

bioRxiv preprint doi: https://doi.org/10.1101/2021.04.14.439704; this version posted April 14, 2021. The copyright holder for this preprint (which was not certified by peer review) is the author/funder. All rights reserved. No reuse allowed without permission.

Methods

Patient-derived BTSC cultures

The human BTSC lines 112 and 172 were generously provided by Dr. Keith Ligon at Harvard Medical School. BTSC lines were generated following surgery with informed consent of adult glioblastoma patients following the BWH/Partners IRB protocol for use of excess/discarded tissue at Harvard University. BTSCs 12, 30, 50, 68, 73, and 147 were provided by Dr. Samuel Weiss at the University of Calgary. Cells were characterized for major mutations in glioblastoma including EGFRvIII, p53, PTEN, and IDH1 status[29]. BTSCs 68, 73, 147, and 172 that naturally harbour EGFRvIII mutations, and BTSCs 12, 30 and 50 that do not harbour the mutation, were used in this study. Prior to use, BTSCs were recovered from cryopreservation in 10% dimethyl sulfoxide and cultured in Nunc ultra-low attachment flasks as neurospheres in NeuroCult NS-A medium (Stemcell Technologies, #05750) supplemented with 100 U/mL penicillin, 100 µg/mL streptomycin (Sigma Aldrich, #P4333), heparin (2 µg/mL, Stemcell Technologies, #07980), human EGF (20 ng/mL, Miltenyi Biotec, #130-093-825), and human FGF (10 ng/mL, Miltenyi Biotec, #130-093-838). All cell lines were tested negative for mycoplasma.

Generation of transgenic BTSCs

We employed 3 different approaches to delete *LGALS1* in patient-derived human BTSCs. First, genetic deletion of *LGALS1* was achieved using CRISPR. Briefly, two gRNAs were designed using off-spotter software to delete exon 2-4 resulting in a 2.673 kb deletion of *LGALS1* gene. gRNA-1 and -2 were cloned into pL-CRISPR.EFS.GFP and pL-CRISPR.EFS.tRFP, respectively. 5 ug of each construct were nucleofected into BTSC73 and BTSC147 using an AMAXA nucleofector 2b device (Lonza, #AAB-1001). The GFP and RFP positive cells were then sorted two days post-electroporation and plated clonally using FACSAria Fusion. Genomic DNA was isolated from each clone and screened for *LGALS1* deletion via PCR using specific internal and external primers around the site of the deletion. This led to the identification of monoallelic deletion, biallelic deletion and non-deletion clones. *LGALS1* mRNA and protein levels were analyzed by RT-qPCR and WB, respectively, to assess KD levels (**Supplementary Fig. 3**). The following gRNAs and screening primers were used for CRISPR/Cas9 system:

bioRxiv preprint doi: https://doi.org/10.1101/2021.04.14.439704; this version posted April 14, 2021. The copyright holder for this preprint (which was not certified by peer review) is the author/funder. All rights reserved. No reuse allowed without permission.

gRNA-1-*LGALS1*:	caccGGAGAGTGCCTTCGAGTGCG
gRNA-1- *LGALS1*-Rc:	aaacCGCACTCGAAGGCACTCTCC
gRNA-2- *LGALS1*:	caccGCCTCCAGGTTGAGGCGGTT
gRNA-2- *LGALS1*-Rc:	aaacAACCGCCTCAACCTGGAGGC
LGALS1 External-Fwd:	CTTGGCTTGGTCAGAGGATGC
LGALS1 External-Rev:	TTCAGAGGGAGCAGAGGCAG
LGALS1 Internal-Fwd:	TCAAGAATCAAGCGAGCCC
LGALS1 Internal-Rev:	CAGTATCCCATGAACGCACC

Second, the transgenic *LGALS1* KD BTSCs were generated via lentivirus carrying two different *LGALS1* shRNA plasmids (Origene, #TL31756). *LGALS1* KD BTSC73 lines were established by antibiotic selection (0.5 µg/mL puromycin). As control, a lentivirus carrying a non-targeting construct was used.

Third, we conducted transient KD of *LGALS1* using siRNA approach. ON TARGET-plus SMART pool human *LGALS1* siRNA (Dharmacon, #L-011718-00-0005) and ON TARGET-plus non-targeting pool (Dharmacon, #D-001810-10-05) were used. siRNA (100 nM) were nucleofected into BTSCs (10^6 cells) and cultured in BTSC media at 37°C in a humidified atmosphere of 5% CO_2.

Transient KD of *HOXA5*, *STAT3* and *EGFR*/*EGFRvIII* was achieved using siRNA approach. ON TARGET-plus SMART pool human *HOXA5* siRNA (Dharmacon, #L-017574-00-0005), *STAT3* siRNA (Dharmacon, #L-003544-00-0005) and *EGFR*/*EGFRvIII* siRNA (Dharmacon, #L-003114-00-0005) were used. siRNA (100 nM) were nucleofected into BTSCs (10^6 cells) and cultured in BTSC media at 37°C in a humidified atmosphere of 5% CO_2.

Mouse astrocytes culture

Stat3 floxed (*Stat3*$^{loxP/loxP}$) astrocyte line was generated from mice with floxed *Stat3* alleles (*Stat3*$^{loxP/loxP}$)[11]. To generate Stat3 KO (Stat3$^{-/-}$), the genes flanked by loxP sites were excised *in vitro* using adenovirus encoding the recombinase Cre (University of Lowa). MSCV-EGFRvIII-expressing astrocytes were generated by retroviral mediated delivery of MSCV-EGFRvIII plasmids into *Stat3*$^{loxP/loxP}$ astrocytes, and were immortalized by retroviral-mediated expression of the SV40 large T antigen protein as described[11].

bioRxiv preprint doi: https://doi.org/10.1101/2021.04.14.439704; this version posted April 14, 2021. The copyright holder for this preprint (which was not certified by peer review) is the author/funder. All rights reserved. No reuse allowed without permission.

Inhibitors

EGFR and EGFRvIII activity were inhibited by lapatinib (Sigma, #CDS022971). STAT3 was inhibited using WP1066 (Sigma, #573097) and S3I-201 (Sigma, #SML0330). OTX008 (MedChemExpress, #HY-19756) was used to inhibit galectin1.

Ionizing radiation

For ELDA and measurement of cell death, BTSCs were dissociated to single cell suspension using Accumax (Innovative Cell Technologies, #AM105). BTSCs were plated and irradiated with either 4 or 8 Gy using the X-Ray Irradiation System (Faxitron MultiRad 225).

OTX008 treatment

For LDA, ELDA and measurement of cell death, BTSCs were dissociated to single cell suspension, plated and treated with the indicated OTX008 concentrations or vehicle for 7 days.

Limiting dilution assay and extreme limiting dilution assay

For LDA, BTSCs were dissociated to single cell suspension using Accumax, counted and plated in 96-well plate at different densities ranging from 200 to 6 cells per well in triplicates. Spheres were counted 7 days after plating.

For ELDA experiments, decreasing numbers of BTSCs per well (dose: 25, 12, 6, 3 and 1) were plated in a 96-well plate with a minimum of 12 wells/dose. Seven days after plating, the presence of spheres in each well was recorded and analysis was performed using the software available at http://bioinf.wehi.edu.au/software/elda/[44].

Cell population growth assay

BTSCs were dissociated to single cell suspension using Accumax, counted and 2 x 10^4 cells were plated. After 24-, 48-, 72- and 96 h, live cells were counted by trypan blue exclusion with Countess™ II FL Automated Cell Counter.

EdU proliferation assay

bioRxiv preprint doi: https://doi.org/10.1101/2021.04.14.439704; this version posted April 14, 2021. The copyright holder for this preprint (which was not certified by peer review) is the author/funder. All rights reserved. No reuse allowed without permission.

BTSCs were dissociated to single cell suspension using Accumax, counted and 10^6 cells were plated and incubated with 10 µM EdU. After 22h, BTSCs were fixed, permeabilized and stained using the Click-iT™ EdU cell proliferation kit (ThermoFisher, #C10337) according to the manufacturer's protocol. Fluorescence was analyzed by flow cytometry (BD FACS CantoII) and images were acquired using a 10X objective on an Olympus IX83 microscope with an X-Cite 120 LED from Lumen Dynamics and an Olympus DP80 camera. Data were analyzed using the FlowJo software. The proportion of cells that incorporated EdU was determined as the ratio of EdU positive cells to the total number of cells.

Cell cycle analysis

BTSCs were dissociated to single cell suspension using Accumax, counted and 10^6 cells were plated. After 22h, cells were dissociated to single cell suspension, harvested and fixed with 70% of ethanol overnight at 4°C. The cells were washed with PBS and stained with FxCycle™ PI/RNase staining solution (ThermoFisher, #F10797). The fluorescence was analyzed by flow cytometry (BD FACS CantoII). The fraction of G0/G1, S and G2 phase cells was calculated using the FlowJo software.

Cell viability and cell death assessment

BTSCs were dissociated to single cell suspension using Accumax and seeded at a density of 200 cells/well, in a 96-well plate. Cell viability was evaluated 7 days post-plating using CellTiter-Glo® Luminescent Cell Viability Assay (Promega, #G7570) according to the manufacturer's protocol. Briefly, CellTiter-Glo reagent was added to the culture media. After 2 min under orbital agitation, luminescence was recorded. The luminescent signal is proportional to the amount of ATP present and directly proportional to the number of cells present in culture.

BTSCs cell death was evaluated 48 h following IR and 7 days following OTX008 treatment. Cell death was determined using TACS annexin V-FITC apoptosis detection kit (R&D systems 4830-01-K) according to the manufacturer's protocol. Briefly, 10^6 cells were seeded in a 25 cm^2 flask. Co-staining with TACS annexin V-FITC and propidium iodide (PI) (R&D, #4830-01-K) was performed on single cells suspension following the manufacturer's instructions. The fluorescence was analyzed by flow cytometry (BD FACS CantoII). Data were analyzed using

bioRxiv preprint doi: https://doi.org/10.1101/2021.04.14.439704; this version posted April 14, 2021. The copyright holder for this preprint (which was not certified by peer review) is the author/funder. All rights reserved. No reuse allowed without permission.

the FlowJo software. Both early apoptotic (annexin V-positive, PI-negative) and late apoptotic (annexin V-positive and PI-positive) cells were included in the cell death plots.

Protein immunoprecipitation

Immunoprecipitations were performed from whole cell lysate of BTSCs. Cells were lysed for 30 min on ice in lysis buffer (50 mM Tris pH 7.5, 150 mM NaCl, 2 mM $MgCl_2$, 0.5 mM EDTA, 0.5% Triton X-100, protease inhibitor cocktail). Lysates were cleared by centrifugation (14,800 *g*, 20 min, 4°C) and subsequently incubated with either anti-HOXA5 antibody (Abcam, ab82645) or rabbit IgG (Cell Signaling, #3900S) as a control. Primary antibody incubations were carried out overnight at 4°C, followed by a 1 h incubation at room temperature with Dynabeads Protein G magnetic beads (Thermo Fisher Scientific, #10003D). Beads were washed three times with lysis buffer and eluted by boiling in SDS sample buffer. Immunoprecipitates were analyzed by immunoblotting using the indicated antibodies.

Immunoblotting and antibodies

Total proteins were harvested in RIPA lysis buffer containing protease and phosphatase inhibitors (Thermo Fisher Scientific, #A32959). Protein concentration was determined by Bradford assay (Bio-Rad), after which samples were subjected to SDS-PAGE and electroblotted onto Immobilon-P membrane (Millipore). Membranes were blocked in 5% bovine serum albumin in TBST, before sequential probing with primary antibodies and HRP-conjugated secondary antibodies in blocking solution. Target proteins were visualized by ECL (Biorad) using ChemiDoc Imaging System (Biorad). The following antibodies were used: galectin1 (1:1000, Cell Signaling, #12936), HOXA5 (1:500, Abcam, # ab82645), phospho-EGFR (Tyr1068) (1:1000, Abcam, # ab40815), EGFR (1:1000, Abcam, # ab32077), α-tubulin (1:5000, Abcam, #4074), STAT3 (1:1000, Cell Signaling, #9139) and phospho-STAT3 (TyrY705) (1:1000, Cell Signaling, #9138).

Immunofluorescence

For immunostaining, BTSCs were plated on Lab-Tek II, CC2-treated chamber slide system (Thermo Fisher Scientific, #154941) in media containing 10% FBS, for 30 min. Cells were washed with PBS and fixed with 4% paraformaldehyde for 15 min at room temperature. Next,

bioRxiv preprint doi: https://doi.org/10.1101/2021.04.14.439704; this version posted April 14, 2021. The copyright holder for this preprint (which was not certified by peer review) is the author/funder. All rights reserved. No reuse allowed without permission.

cells were permeabilized with 0.5% Triton X-100 (Sigma Aldrich, #T8787) for 20 min and blocked for 1 h with 5% normal donkey serum (NDS) in 1X-PBS. The cells were then incubated overnight at 4 °C with primary antibodies to galectin1 (1:100, Cell Signaling, #12936S) diluted in 5% NDS-1X PBS. Cells were washed with PBS and then incubated with secondary Alexa fluor 488 goat anti-rabbit (1:500, Cell Signaling, #4412 s) antibody for 1 h. 2 µg/mL DAPI (Thermo Fisher Scientific, #D1306) was used to detect the nuclei and ProLong Gold Antifade Mountant (Thermo Fisher Scientific, #P36934) was used for mounting. Images were captured using a 63X objective on a laser scanning confocal microscope (ZEISS LSM 800).

Duolink proximity ligation assay

PLAs were performed using a Duolink In Situ Red Starter Kit (Sigma, #DUO92101) according to the manufacturer's instructions. Briefly, BTSC were plated on Lab-Tek II, CC2-treated chamber slides in media containing 10% FBS, for 30 min. Cells were washed with PBS and fixed with 4% paraformaldehyde for 15 min at room temperature. Next, cells were permeabilized with 0.5% Triton X-100 for 20 min, blocked using Duolink blocking solution, and then incubated with primary antibodies at 4 °C overnight. After washing, the oligonucleotide (Minus and Plus)-conjugated secondary antibodies were added and incubated for 1 h at 37 °C. Subsequently, cells were washed and incubated with the ligation solution for 30 min at 37 °C. The ligated nucleotide circles were amplified using polymerase via the addition of the amplification solution followed by incubation for 100 min at 37 °C. The slides were washed briefly, and Duolink In Situ Mounting Medium with DAPI (DUO82040, Sigma) was added to each sample to stain the nuclei. The visualized fluorescence PLA signals were captured using a 63X objective on a laser scanning confocal microscope (ZEISS LSM 800).

Whole-transcriptome analyses (RNA-seq)

Total RNAs were isolated from cells using TRIzol reagent (Invitrogen) according to the manufacturer's instructions. The quality of RNA was assessed by bioanalyzer before sequencing. Libraries for poly(A)$^+$ RNA were prepared according to the Illumina protocol. Libraries were sequenced on Illumina GAIIX Genome Analyzer or on HI-SEQ 2000 platforms. RNA-seq reads were mapped to the human genome assembly (hg38) using HISAT2. The number of aligned reads per gene was obtained with HTSeq and gene annotations were

bioRxiv preprint doi: https://doi.org/10.1101/2021.04.14.439704; this version posted April 14, 2021. The copyright holder for this preprint (which was not certified by peer review) is the author/funder. All rights reserved. No reuse allowed without permission.

retrieved from GENCODE. Genes with an average read counts smaller than 10 were filtered out. Differential expression analysis was performed with DESeq2, *p*-values were corrected by independent hypothesis weighting[51,52]. Genes with an adjusted *p*-value smaller than 0.1 were considered statistically differentially expressed. Gene Set Enrichment Analysis was done with the fgsea R package. The Log fold changes from DESeq2 were used to create a pre-ranked gene-list. The Reactome database was used as a reference for pathways.

Gene expression analysis

Total RNAs were isolated from cells using TRIzol reagent (Invitrogen) according to the manufacturer's instructions. RNAs were then subjected to reverse transcription using the 5X All-In-One RT MasterMix cDNA synthesis system (abm, #G492). Real-time quantitative polymerase chain reaction (RT-qPCR) was performed using the fluorescent dye SYBR Green (Biorad, #1725271). mRNA expression levels were then normalized to the housekeeping gene beta-glucuronidase (GUSB).

The following qPCR primers were used:

GUSB-Fwd:	GCGTTCCTTTTGCGAGGAGA
GUSB-Rev:	GGTGGTATCAGTCTTGCTCAA
PIM2-Fwd:	GTGGCTGTGCCAAACTCATT
PIM2-Rev:	ATGCCCAGTGACCAGACAGT
E2F7-Fwd:	GAAAGCACCAAAGAGCCTTCT
E2F7-Rev:	AAGACCATGCAAGGGACACT
NEDD9-Fwd:	TGACTGTAGCAGCAGTGATGG
NEDD9-Rev:	TGTTCCAGCTGCATCTTGTT
MCM5-Fwd:	CAGAGGCAGATGTGGAGGAG
MCM5-Rev:	GCTTGAGCTGCTTCTCGATG
KLHL22-Fwd:	CCACAATGACCTGAATGCTG
KLHL22-Rev:	TCAGGTAATCCTCCCCTCTG
NDC80-Fwd:	CTGTTAACCAGGGGCTCAGT
NDC80-Rev:	GACCCAACATGTGTAGCAACC
GSPT2-Fwd:	CAAAGATATGGGCACTGTGG
GSPT2-Rev:	GTTTTCACCTGGGGCTACAA

bioRxiv preprint doi: https://doi.org/10.1101/2021.04.14.439704; this version posted April 14, 2021. The copyright holder for this preprint (which was not certified by peer review) is the author/funder. All rights reserved. No reuse allowed without permission.

SPC24-Fwd:	CACCAGAGAGCTGGAAGAGC
SPC24-Rev:	TCCCTGGCTCACACTCATAA
HIRA-Fwd:	ACGCACGGTACCTCGTAAAC
HIRA-Rev:	TGTTGACTCCCACTGGCTTC
SMARCA4-Fwd:	GATGACAGTGAAGGCGAGGA
SMARCA4-Rev:	GGCCAAGCTTGATCTTCACTT
CENPM-Fwd:	TCTTGGGGAAGGTGTGTTTC
CENPM-Rev:	TAGAGCAGGGGGCTTTGATA
GTSE1-Fwd:	CAGAAGTAGCTCGGGAGGAA
GTSE1-Rev:	CTTGCAGCATCTGGAGTGAC
MAD2L2-Fwd:	GCTGTACCTTCACAGTCCTGGT
MAD2L2-Rev:	ATGTCCGACGTCATGGTTTT
NEK6-Fwd:	GACGCCCTACTACATGTCACC
NEK6-Rev:	TGGCACAGGGAGAAGAGATT
SKP2-Fwd:	ACCTTTCTGGGTGTTCTGGA
SKP2-Rev:	CTGGGTGATGGTCTCTGACA
CCND3-Fwd:	ATTTCCTGGCCTTCATTCTG
CCND3-Rev:	CGGGTACATGGCAAAGGTAT
CDK6-Fwd:	CATTCAAAATCTGCCCAACC
CDK6-Rev:	GGTGGGAATCCAGGTTTTCT
CDKN2D-Fwd:	GTCATGATGTTTGGCAGCAC
CDKN2D-Rev:	CGTCATGGACTGGACTGGTA

Chromatin immunoprecipitation

Cells were washed with PBS containing protease inhibitors (Thermo Fisher Scientific, #A32959) before fixation. Cells were cross-linked with 1% formaldehyde in PBS for 10 min, and quenched with a solution containing 0.125 M glycine in PBS for 5 min at room temperature. Washing, fixing and quenching of the cells were performed in 15-ml Falcon tubes with cells rotating at room temperature. Following quenching, cells were washed twice with PBS containing protease inhibitors, and cell pellets were collected by spinning at 150 *g*. for 10 min at 4 °C. Pellets were dissolved in ChIP lysis buffer (40 mM Tris-HCl, pH 8.0, 1.0% Triton

bioRxiv preprint doi: https://doi.org/10.1101/2021.04.14.439704; this version posted April 14, 2021. The copyright holder for this preprint (which was not certified by peer review) is the author/funder. All rights reserved. No reuse allowed without permission.

X-100, 4 mM EDTA and 300 mM NaCl) containing protease inhibitors. Chromatin was fragmented by sonication in a water bath Bioruptor at 4 °C to an average length of 500 base pairs (bp). The lysates were spun at 12,000 *g*. for 15 min, and the supernatant was diluted 1:1 in ChIP dilution buffer containing 40 mM Tris-HCl, pH 8.0, and 4 mM EDTA plus protease inhibitors. Immunoprecipitation was done using a ChIP-grade HOXA5 antibody (Abcam, # ab82645), total STAT3 antibody (Cell Signaling Technology, 9139), mouse IgG antibody (Cell Signaling, 5415S), or rabbit IgG antibody (Cell Signaling, #3900S). Antibody-protein-DNA complexes were collected, washed and eluted, and the cross-links were reversed as described previously[53]. Immunoprecipitated DNA was analyzed by q-PCR and binding enrichment was expressed as % of input. The following primer sequences were used:

OSMR-Fwd:	GACTGAAGGGAGGGAATTCCTGT
OSMR-Rev:	CAATTTCCCGTCTTGCTG
LGALS1-a-Fwd:	ACTTGTGGGCCTAGCTCATC
LGALS1-a-Rev:	TTCTCCATCCCTCTCCA
LGALS1-b-Fwd:	GCCACTCTGATTGGTCACCT
LGALS1-b-Rev:	ACGCTCCCACCCTTTTAACT
HPRT-Fwd:	CGGTAGGTTTGGGAATCA
HPRT-Rev:	CAGTTTGCAGGCTCACTA
ARIDA5B-Fwd:	GCGCTGGGTTATATAAACACATTA
ARIDA5B-Rev:	AAATGCGAGAAGCGAGTCTG
DSCAM-Fwd:	AAGGGGCTATATGTTTGGGATT
DSCAM-Rev:	CTCCTTCCAAATCCTTGCTG
EDN1-Fwd:	GGGCAGGTTTAGCAAAGGTC
EDN1-Rev:	TTAGTCACCAACAGGCAACG
KCNK2-Fwd:	CGTGGATGCTTCGTGTGTAA
KCNK2-Rev:	TTCAGGAAGAAATTCCCTGATT
ACSS3-Fwd:	TTGAATATATCTCCTCTTATGACCAC
ACSS3-Rev:	AGATCAGCTTTTTGCTTCTTTG
HBB-Fwd:	CTGTTTGAGGTTGCTAGTG
HBB-Rev:	TCATCACTTAGACCTCACC

bioRxiv preprint doi: https://doi.org/10.1101/2021.04.14.439704; this version posted April 14, 2021. The copyright holder for this preprint (which was not certified by peer review) is the author/funder. All rights reserved. No reuse allowed without permission.

Transcription factor binding sites enrichment analysis

Transcription factor binding sites over-representation analysis was performed using oPOSSUM (v.3.0, Single Site Analysis tool). Deferentially downregulated genes were used as targets and all genes measured by our RNA-seq were used as background (Conservation cutoff: 0.6; Matrix score threshold: 85%; upstream/downstream region: 5kb/5kb; JASPAR CORE Profiles: All vertebrate profiles).

Human glioblastomas and gene-survival analysis

Patient and expression data was retrieved from TCGA (Agilent, G4502A)[54]. Patients were divided into High and Low groups by expression of *HOXA5* and *LGALS1* (separated at the median) and if they were treated with radiotherapy (+/-). Overall and progress-free survival was analyzed by Kaplan-Meier curves. Pairwise comparisons between groups, using a log-rank test, were corrected with Benjamini-Hochberg multiple testing procedure. Adjusted *p*-values smaller than 0.1 were considered statistically significant.

ChIP-seq analysis

HOXA5 ChIP-seq reads from colon adenocarcinoma (GSE51142) were mapped to the human genome assembly (hg38) using Bowtie2[47]. Peak calling was carried out using MACS (with thresholds p-value < 10^{-5} and FDR < 0.2). Averaged conservation scores for HOXA5 ChIP-seq peaks were calculated based on phastcon scores (0~1; UCSC 30-way). Transcription start sites were obtained from bioMart. Peak height was calculated as the number of tags per 100 bp. Distance between TSS and ChIP-seq summit was calculated using Bedtools.

Dual-luciferase Reporter Assay

The upstream 376 bp region of the human *LGALS1* transcriptional start site was cloned into the pGL4.23 (Promega) vector to generate the *LGALS1* luciferase reporter gene (*LGALS1* pGL4.23) by digesting the plasmid and the annealed primer pair using EcoRV (NEB, #R0195L) and HindIII (NEB, #R0104L) and ligating them with T4 DNA ligase (NEB, #M0202L). The following primer sequences were used: Fwd; CTCAGCCATCTTCTCTGGGC; Rev: AGTTAAAAGGGTGGGAGCGT. The construct was confirmed by DNA sequencing. BTSCs and mouse astrocytes were electroporated with the *LGALS1* pGL4.23 construct or the empty

bioRxiv preprint doi: https://doi.org/10.1101/2021.04.14.439704; this version posted April 14, 2021. The copyright holder for this preprint (which was not certified by peer review) is the author/funder. All rights reserved. No reuse allowed without permission.

pGL4.23. Luciferase assays were performed 48 h after transfection with the Dual-Luciferase Reporter Assay system (Promega, #E1910) with a GloMax Luminometer (Promega). In all experiments, cells were electroporated with a Renilla firefly reporter control and the firefly luminescence signal was normalized to the Renilla luminescence signal.

Stereotaxic injections and bioluminescent imaging

All animal experiments were conducted under the institutional guidelines and were approved by McGill University Animal Care Committee (UACC). Housing room temperature and relative humidity were adjusted to 22.0 ± 2.0 °C and 55.0 ± 10.0%, respectively. The light/dark cycle was adjusted to 12 h lights-on and 12 h lights-off. Autoclaved water and irradiated food pellets (Tecklad, #2918) were given ad libitum. For intracranial injections, 3×10^5 luciferase-expressing BTSCs were stereotactically implanted into the right striata (0.8 mm lateral to the bregma, 1 mm dorsal and 2.5 mm from the pial surface) of randomized 8-week-old male SCID mice. Mice were randomly assigned to the treatment or vehicle. For OTX008 treatment, seven days post BTSCs injection, mice were administered intraperitoneally 10 mg/kg OTX008 or vehicle control every two days. For IR treatment, mice received 4 Gy of IR using the X-Ray Irradiation System (Faxitron MultiRad 225) five and ten days following BTSCs injections[55]. To examine tumour volume, the animals were intraperitoneally injected with 200 µL of 15 mg/mL D-luciferin (Thermo Fisher Scientific, #88292), anesthetized with isoflurane inhalation, and subjected to bioluminescence imaging with a CCD camera (IVIS, Xenogen) on a weekly basis. All bioluminescent data were collected and analyzed using IVIS software. For Kaplan-Meier survival plots, mice were collected when they showed signs of tumour-related illness.

Subcutaneous xenografts

Luciferase-expressing BTSCs (10^6 cells) were subcutaneously injected into flanks of 8-week-old male SCID mice. Mice were randomly assigned to the treatment or vehicle. For OTX008 treatment, seven days post BTSCs injection, mice were administered intraperitoneally 10 mg/kg OTX008 or vehicle control every two days. Tumour growth was evaluated by luciferase imaging. Mice were killed when mice developed neurological signs and ulcerated tumours, and the tumours were removed and weighted.

bioRxiv preprint doi: https://doi.org/10.1101/2021.04.14.439704; this version posted April 14, 2021. The copyright holder for this preprint (which was not certified by peer review) is the author/funder. All rights reserved. No reuse allowed without permission.

Statistical analysis

Statistical analysis was performed using ANOVA and Student's *t*-test, with the aid of GraphPad software 7. Two-tailed and unpaired t-tests were used to compare two conditions. One-way ANOVA with Tukey's or Dunnett's post hoc analyses were used for analyzing multiple groups. Data are shown as mean with standard error of mean (mean ± SEM). The log-rank test was used for statistical analysis in the Kaplan-Meier survival plot. *p*-values of equal or less than 0.05 were considered significant and were marked with an asterisk on the histograms. *p*-values of less than 0.05 are denoted by *, *p*-values of less than 0.01 are denoted by **, and *p*-values of less than 0.001 are denoted by *** on the histograms.

bioRxiv preprint doi: https://doi.org/10.1101/2021.04.14.439704; this version posted April 14, 2021. The copyright holder for this preprint (which was not certified by peer review) is the author/funder. All rights reserved. No reuse allowed without permission.

Acknowledgements

This work was supported by grants from the Canadian Institute of Health Research and Cancer Research Society. AJA is an Fonds de la recherche en santé du Québec (FRQS) scholar in Glioblastoma Biology. AB is supported by an FRQS postdoctoral fellowship. We thank Dr. Samual Weiss at the University of Calgary for sharing BTSC12, 30, 50, 68, 73,147 and Dr. Keith Ligon at Harvard Medical School for the generation of BTSC112 and 172. We thank Mehdi Haghi for technical assistance. We thank staff at the Lady Davis Institute Animal Core Facility and Christian Young at Fluorescence-Activated Cell Sorting (FACS) facility at the Lady Davis Institute for Medical Research – Jewish General Hospital for their help with our studies.

bioRxiv preprint doi: https://doi.org/10.1101/2021.04.14.439704; this version posted April 14, 2021. The copyright holder for this preprint (which was not certified by peer review) is the author/funder. All rights reserved. No reuse allowed without permission.

Figure legends

Fig. 1. Galectin1 is a direct transcriptional target of EGFRvIII/STAT3 in patient-derived BTSCs.

(**a**) Patient-derived BTSCs that harbour EGFRvIII mutation or lack the mutation were analyzed by immunoblotting using the antibodies indicated on the blots. Wild type EGFR and EGFRvIII bands are marked with * and **, respectively. Tubulin was used as a loading control. (**b-c**) KD of *EGFR*/*EGFRvIII* in BTSCs was induced by electroporation using siRNA. KD and control BTSCs (siCTL) were analyzed by immunoblotting as described in a. (**d-g**) BTSCs were treated with 1-5 µM lapatinib and galectin1 expression were assessed by immunoblotting (d-e) and immunostaining (f-g). Nuclei were stained with DAPI. Images were obtained with a 63X objectives on a laser scanning confocal microscope (ZEISS LSM 800). Scale bar = 10 µm. (**h**) Putative STAT3 binding sites at positions -300, -135 and -72 bp upstream of the *LGALS1* gene transcriptional start site (TSS) are shown. (**i**) BTSCs were analyzed by immunoblotting using the antibodies indicated on the blots as described in a. (**j-k**) KD of *STAT3* was induced in BTSC73 (**j**) and BTSC147 (**k**) via electroporation using siRNAs. *STAT3* KD and control BTSCs were analyzed by immunoblottig as described above. (**l-o**) BTSCs were subjected to immunoblotting or immunostaining following treatment with 25- 50 µM of the STAT3 inhibitor, S3I-201. Images were captured as described in f-g. Scale bar = 10 µm. (**p-r**) EGFRvIII-expressing BTSCs were subjected to ChIP using an antibody to STAT3 or IgG control followed by RT-qPCR for *LGALS1* promotor region using two different pairs of primers (*LGALS1*-a and *LGALS1*-b). *OSMR*, and *HPRT* loci were used as positive and negative controls, respectively. BTSC73 (**p**): $*p_{OSMR} = 0.0288$, $**p_{LGALS1\text{-a}} = 0.0079$, $**p_{LGALS1\text{-b}} = 0.0013$; Unpaired two-tailed *t*-test, n = 3; BTSC172 (**q**): $***p_{OSMR} = 0.0002$, $*p_{LGALS1\text{-a}} = 0.0168$, $*p_{LGALS1\text{-b}} = 0.0102$; Unpaired two-tailed *t*-test, n = 3; BTSC112 (**r**): $*p_{OSMR} = 0.0450$, $***p_{LGALS1\text{-a}} = 0.0007$, $*p_{LGALS1\text{-b}} = 0.0256$; Unpaired two-tailed *t*-test, n = 3. (**s**) *STAT3* KD and control BTSCs were electroporated with a luciferase reporter plasmid driven by a promoter containing 376 bp region upstream of the *LGALS1* gene TSS (*LGALS1* pGL4.23) or the control pGL4.23-basic reporter plasmid (pGL4.23) together with a Renilla expression plasmid and were subjected to dual luciferase assay. $***p < 0.0001$ for each pairwise comparison except: $*p_{\text{si}STAT3\ (LGALS1\ \text{pGL4.23 vs. pGL4.23})} = 0.0311$; One-way ANOVA followed by Tukey's test for multiple comparisons, n = 3. (**t**) Luciferase reporter assay was performed in BTSC73 following treatment of the cells with

bioRxiv preprint doi: https://doi.org/10.1101/2021.04.14.439704; this version posted April 14, 2021. The copyright holder for this preprint (which was not certified by peer review) is the author/funder. All rights reserved. No reuse allowed without permission.

STAT3 inhibitors, 5 µM WP1066 and 50 µM S3I-201, as described in S. ***$p < 0.0001$ for each pairwise comparison except: *$p_{\text{WP1066 (}LGALS1\text{ pGL4.23 vs. pGL4.23)}} = 0.0301$; One-way ANOVA followed by Tukey's test for multiple comparisons, n = 3. Data are presented as the mean ± SEM, n = 3 independent biological cell cultures.

Fig. 2. Galectin1 controls the growth of EGFRvIII-expressing BTSCs.
(**a-b**) Cell viability was assessed by CellTiter-Glo assay in *LGALS1* CRISPR and control (CTL) BTSCs. BTSC73 (**a**): ***$p < 0.0001$; BTSC147 (**b**): ***$p = 0.0003$; Unpaired two-tailed *t*-test, n = 3. (**c**) Population growth curves for *LGALS1* CRISPR and CTL BTSC73 are shown. **$p = 0.064$; Unpaired two-tailed *t*-test, n = 3. (**d-e**) BTSCs were treated with 1 or 10 µM OTX008 and cell viability was assessed by CellTiter-Glo assay. BTSC73 (**d**): ***$p_{\text{CTL vs. OTX008 1 µM}} = 0.0007$, ***$p_{\text{CTL vs. OTX008 10 µM}} = 0.0001$; BTSC147 (**e**): **$p_{\text{CTL vs. OTX008 1 µM}} = 0.002$, ***$p_{\text{CTL vs. OTX008 10 µM}} = 0.0001$; One-way ANOVA followed by Dunnett's test, n = 3. (**f**) Population growth curves of BTSC73 treated with 1 or 10 µM OTX008 are shown. ***$p_{\text{CTL vs. OTX008 1 µM}} = 0.0003$, ***$p_{\text{CTL vs. OTX008 10 µM}} = 0.0001$; One-way ANOVA followed by Dunnett's test, n = 3. (**g**) Representative images of EdU staining in *LGALS1* CRISPR and CTL BTSC73 are shown. (**h**) The number of EdU positive cells was quantified using ImageJ software, ***$p = 0.0001$; Unpaired two-tailed *t*-test, n = 3. (**i**) EdU incorporation was analyzed by flow cytometry in *LGALS1* CRISPR and CTL BTSC73. Representative scatter plots of flow cytometry analyses are shown. Data are presented as the mean ± SEM, n = 3 independent biological cell cultures.

Fig. 3. Galectin1 controls the tumourigenic capacity of EGFRvIII-expressing BTSCs.
(**a-b**) *LGALS1* CRISPR or CTL BTSC73 were injected into 8 week-old SCID mice and allowed to form tumours subcutaneously. Representative bioluminescence real-time images tracing BTSCs and tumour growth are shown (**a**). Graph represents tumour mass for each group (**b**): ***$p = 0.0002$; Unpaired two-tailed *t*-test, n = 4 mice for each group. (**c-f**) BTSC73 or BTSC147 were injected subcutaneously into 8 week-old SCID mice and then treated with 10 mg/kg OTX008. Representative bioluminescence real-time images tracing BTSCs and tumour growth are shown (**c, e**). Graph represents tumour mass for each group (**d**): ***$p = 0.0002$; Unpaired two-tailed *t*-test, n ≥ 6 mice for each group. (**f**): ***$p = 0.0008$; Unpaired two-tailed *t*-test, n = 5 mice for each group. (**g-j**) *LGALS1* CRISPR or CTL BTSC73 (3×10^5 cells per brain) were

bioRxiv preprint doi: https://doi.org/10.1101/2021.04.14.439704; this version posted April 14, 2021. The copyright holder for this preprint (which was not certified by peer review) is the author/funder. All rights reserved. No reuse allowed without permission.

intracranially injected into 8 week-old SCID mice, n = 6 mice for each group. Representative bioluminescence real-time images tracing BTSCs and tumour growth are shown (**g**). Intensities of luciferase signal were quantified at different time points using Xenogen IVIS software (**h**): $^{**}p = 0.0041$. Graph represents quantification of animal weight from day 1 to day 28 (**i**): $^{***}p_{21days} = 0.0004$, $^{***}p_{28days} < 0.0001$; Unpaired two-tailed *t*-test. Kaplan–Meier survival plot was graphed to evaluate mice lifespan in each group, mice were collected at the end stage. $p = 0.0011$; Two-sided log-rank test, n = 6 mice (**j**). Data are presented as the mean ± SEM.

Fig. 4. Genome wide analysis of *LGALS1*-differentially regulated genes.

(**a**) *LGALS1* CRISPR and CTL BTSC73 were subjected to RNA-seq analysis, n = 3 independent replicates. Volcano plot representing the differentially regulated genes in *LGALS1* CRISPR is shown. Up-and down-regulated genes are highlighted in blue and red dots, respectively. Genes with no significant changes in expression are represented as black dots. Black lines show the top genes of the GSEA enriched pathways described in b and c. (**b**) GSEA analysis demonstrates enrichment for Gene Ontology (GO) gene sets corresponding to recruitment of NuMA to mitotic centrosomes. (**c**) GSEA analysis demonstrates enrichment for GO gene sets corresponding to mitotic G2−G2/M phases. (**d-e**) RNA-seq data was validated by RT-qPCR in different EGFRvIII-expressing BTSCs. BTSC73 (**d**): $^{***}p_{LGALS1} = 0.0001$, $p_{SPC24} = 0.2012$, $^{***}p_{E2F7} = 0.0001$, $^{***}p_{GSPT2} = 0.0001$, $^{**}p_{NDC80} = 0.0099$, $^{***}p_{MCM5} = 0.0004$, $^{**}p_{KLHL22} = 0.0028$, $^{**}p_{NEDD9} = 0.0026$, $^{***}p_{PIM2} = 0.0001$, $p_{SMARCA4} = 0.0521$, $^{***}p_{CENPM} = 0.0003$, $^{*}p_{GTSE1} = 0.0194$, $^{*}p_{MAD2L2} = 0.0351$, $p_{NEK6} = 0.5434$, $p_{SKP2} = 0.2693$, $p_{CCND3} = 0.1317$, $^{***}p_{CDKN2D} = 0.0002$, $^{**}p_{CDK6} = 0.0064$; BTSC147 (**e**): $^{***}p_{LGALS1} = 0.0001$, $^{***}p_{SPC24} = 0.0001$, $^{***}p_{E2F7} = 0.0001$, $^{*}p_{GSPT2} = 0.0153$, $^{***}p_{NDC80} = 0.0001$, $^{***}p_{MCM5} = 0.0001$, $^{***}p_{KLHL22} = 0.0006$, $^{**}p_{NEDD9} = 0.0026$, $^{***}p_{PIM2} = 0.0007$, $^{***}p_{SMARCA4} = 0.0001$, $^{***}p_{CENPM} = 0.0001$, $^{***}p_{GTSE1} = 0.0001$, $^{***}p_{MAD2L2} = 0.0002$, $^{**}p_{NEK6} = 0.0029$, $^{***}p_{SKP2} = 0.0009$, $^{***}p_{CCND3} = 0.0001$, $^{***}p_{CDKN2D} = 0.0001$, $^{**}p_{CDK6} = 0.0076$; One-way ANOVA followed by Dunnett's test, n = 3. (**f-i**) Cell cycle distribution was assessed by flow cytometry after PI staining in *LGALS1* CRISPR compared to the corresponding controls in BTSC73 (**f-g**) and BTSC147 (**h-i**). BTSC73 (**g**): $^{***}p_S = 0.0004$, $^{**}p_{G2/M} = 0.0022$; Unpaired two-tailed *t*-test, n = 3. Data are presented as the mean ± SEM.

Fig. 5. Galectin1 controls the self-renewal of the EGFRvIII-expressing BTSCs.

bioRxiv preprint doi: https://doi.org/10.1101/2021.04.14.439704; this version posted April 14, 2021. The copyright holder for this preprint (which was not certified by peer review) is the author/funder. All rights reserved. No reuse allowed without permission.

(**a-b**) *LGALS1* CRISPR and CTL EGFRvIII-expressing BTSCs were subjected to limiting dilution assays (LDA). BTSC73 (**a**): $^{**}p_{200\ cells} = 0.0028$, $^{**}p_{100\ cells} = 0.0016$, $^{**}p_{50\ cells} = 0.0029$, $^{**}p_{25\ cells} = 0.004$, $^{**}p_{12\ cells} = 0.0043$, $^{***}p_{6\ cells} = 0.0001$; BTSC147 (**b**): $^{***}p_{200\ cells} = 0.0005$, $^{**}p_{100\ cells} = 0.0079$, $^{**}p_{50\ cells} = 0.0016$, $^{**}p_{25\ cells} = 0.0039$, $^{**}p_{12\ cells} = 0.0053$, $^{*}p_{6\ cells} = 0.0249$; Unpaired two-tailed *t*-test, n = 3. (**c-d**) EGFRvIII-expressing *LGALS1* CRISPR and CTL BTSCs, BTSC73 (**c**) and BTSC147 (**d**), were subjected to extreme limiting dilution assays (ELDA). (**e-f**) BTSCs that don't harbour the EGFRvIII mutation, BTSC12 (**e**) and BTSC30 (**f**), were electroporated with siCTL or siRNA against *LGALS1* (si*LGALS1*) and subjected to LDA analysis. (**g-h**) BTSCs that don't harbour the EGFRvIII mutation, BTSC12 (**g**) and BTSC30 (**h**), were electroporated with siCTL or si*LGALS1* and subjected for ELDA analysis. (**i-j**) EGFRvIII-expressing BTSCs were subjected to LDA analysis following the treatment with 1 or 10 µM OTX008. BTSC73 (**i**): $^{*}p_{200\ cells\ (CTL\ vs.\ OTX008\ 1\ \mu M)} = 0.0157$, $^{**}p_{200\ cells\ (CTL\ vs.\ OTX008\ 10\ \mu M)} = 0.003$, $^{*}p_{100\ cells\ (CTL\ vs.\ OTX008\ 1\ \mu M)} = 0.0138$, $^{**}p_{100\ cells\ (CTL\ vs.\ OTX008\ 10\ \mu M)} = 0.0022$, $^{*}p_{50\ cells\ (CTL\ vs.\ OTX008\ 10\ \mu M)} = 0.0156$, $^{*}p_{25\ cells\ (CTL\ vs.\ OTX008\ 10\ \mu M)} = 0.0147$, $^{**}p_{12\ cells\ (CTL\ vs.\ OTX008\ 1\ \mu M)} = 0.0028$, $^{**}p_{12\ cells\ (CTL\ vs.\ OTX008\ 10\ \mu M)} = 0.0017$; BTSC147 (**j**): $^{***}p_{200\ cells\ (CTL\ vs.\ OTX008\ 1\ \mu M)} = 0.0004$, $^{***}p_{200\ cells\ (CTL\ vs.\ OTX008\ 10\ \mu M)} = 0.0001$, $^{**}p_{100\ cells\ (CTL\ vs.\ OTX008\ 1\ \mu M)} = 0.0056$, $^{***}p_{100\ cells\ (CTL\ vs.\ OTX008\ 10\ \mu M)} = 0.0007$, $^{*}p_{50\ cells\ (CTL\ vs.\ OTX008\ 1\ \mu M)} = 0.0164$, $^{***}p_{50\ cells\ (CTL\ vs.\ OTX008\ 10\ \mu M)} = 0.001$, $^{*}p_{25\ cells\ (CTL\ vs.\ OTX008\ 10\ \mu M)} = 0.0442$; One-way ANOVA followed by Dunnett's test, n =3. (**k-l**) EGFRvIII-expressing BTSC73 (**k**) and BTSC147 (**l**) were subjected to ELDA analysis following the treatment with 1 or 10 µM OTX008. (**m-n**) EGFRvIII-expressing BTSCs were subjected to LDA analysis following the treatment with 1 or 10 µM OTX008. BTSC68 (**m**): $^{**}p_{200\ cells\ (CTL\ vs.\ OTX008\ 1\ \mu M)} = 0.0059$, $^{**}p_{200\ cells\ (CTL\ vs.\ OTX008\ 10\ \mu M)} = 0.0013$, $^{**}p_{100\ cells\ (CTL\ vs.\ OTX008\ 1\ \mu M)} = 0.0083$, $^{**}p_{100\ cells\ (CTL\ vs.\ OTX008\ 10\ \mu M)} = 0.0017$, $^{**}p_{50\ cells\ (CTL\ vs.\ OTX008\ 1\mu M)} = 0.0069$, $^{**}p_{50\ cells\ (CTL\ vs.\ OTX008\ 10\ \mu M)} = 0.0017$, $^{**}p_{25\ cells\ (CTL\ vs.\ OTX008\ 1\ \mu M)} = 0.0046$, $^{**}p_{25\ cells\ (CTL\ vs.\ OTX008\ 10\ \mu M)} = 0.0022$, $^{**}p_{12\ cells\ (CTL\ vs.\ OTX008\ 1\ \mu M)} = 0.0054$, $^{**}p_{12\ cells\ (CTL\ vs.\ OTX008\ 10\ \mu M)} = 0.0037$; BTSC172 (**n**): $^{**}p_{200\ cells\ (CTL\ vs.\ OTX008\ 10\ \mu M)} = 0.0018$, $^{*}p_{100\ cells\ (CTL\ vs.\ OTX008\ 1\ \mu M)} = 0.015$, $^{**}p_{100\ cells\ (CTL\ vs.\ OTX008\ 10\ \mu M)} = 0.0012$, $^{**}p_{50\ cells\ (CTL\ vs.\ OTX008\ 1\ \mu M)} = 0.0017$, $^{***}p_{50\ cells\ (CTL\ vs.\ OTX008\ 10\ \mu M)} = 0.0001$, $^{*}p_{25\ cells\ (CTL\ vs.\ OTX008\ 10\ \mu M)} = 0.0125$, $^{*}p_{6\ cells\ (CTL\ vs.\ OTX008\ 10\ \mu M)} = 0.0391$; One-way ANOVA followed by Dunnett's test, n = 3. (**o-p**) EGFRvIII-expressing BTSC68 (**o**) and BTSC172 (**p**) were subjected to ELDA analysis following the treatment with 1 or 10 µM OTX008. (**q-r**) BTSCs that don't harbour the EGFRvIII mutation, BTSC12 (**q**) and BTSC30 (**r**), were subjected to LDA analysis following the

bioRxiv preprint doi: https://doi.org/10.1101/2021.04.14.439704; this version posted April 14, 2021. The copyright holder for this preprint (which was not certified by peer review) is the author/funder. All rights reserved. No reuse allowed without permission.

treatment with 1 or 10 μM OTX008. (**s-t**) BTSCs that don't harbour the EGFRvIII mutation, BTSC12 (**s**) and BTSC30 (**t**), were subjected to ELDA analysis following treatment with 1 or 10 μM OTX008. Data are presented as the mean ± SEM.

Fig. 6. Pharmacological inhibition of galectin1 improves the response of BTSC-derived brain tumours to IR.

(**a**) Representative phase-contrast images of irradiated (4 Gy) *LGALS1* CRISPR and CTL BTSC73 are shown. Images were taken following 7 days of plating. Scale bar = 100 μm. (**b**) ELDA was performed following 4 Gy of IR in *LGALS1* CRISPR vs. CTL BTSCs. (**c-d**) *LGALS1* CRISPR and CTL BTSC73 were subjected to IR (8 Gy). Apoptosis analysis was performed by flow cytometry 48 h after IR by annexin V and PI double staining. Representative scatter plots of flow cytometry analyses are shown (**c**). The percentage of cell death (annexin V positive cells) is presented in the histogram (**d**): ***$p_{\text{CTL vs. IR + } LGALS1 \text{ CRISPR}} < 0.0001$, ***$p_{LGALS1 \text{ CRISPR vs. IR + } LGALS1 \text{ CRISPR}} = 0.0003$, **$p_{\text{IR vs. IR + } LGALS1 \text{ CRISPR}} = 0.001$; One-way ANOVA followed by Tukey's test for multiple comparisons, n = 3 independent biological samples. Data are presented as the mean ± SEM. (**e**) Schematic diagram of the experimental procedure in which control BTSC73 (3×10^5 cells per brain) were intracranially injected into randomized Fox Chase SCID mice and then treated with OTX008, 4 Gy of IR or a combination of OTX008 and IR, n = 6 mice for each group. (**f**) Representative bioluminescence real-time images tracing BTSCs and tumour growth are shown. (**g**) Coronal sections of mouse brains were stained with hematoxylin and eosin on day 22 after injection. Representative images of 3 different tumour sections are shown. Scale bar = 1 mm. (**h**) Intensities of luciferase signal were quantified at different time points using Xenogen IVIS software. (**i**) Kaplan-Meier survival plot was graphed to evaluate mice lifespan in each group, mice were collected at the end stage. $p_{\text{CTL vs. IR}} = 0.0896$, $p_{\text{CTL vs. OTX008}} = 0.0117$, $p_{\text{CTL vs. IR + OTX008}} = 0.0177$, $p_{\text{OTX008 vs. IR + OTX008}} = 0.0067$, $p_{\text{IR vs. IR + OTX008}} = 0.0177$; Two-sided log-rank test, n = 6 mice. (**j**) Survival extension of mice bearing BTSC-derived tumours treated with OTX008, IR, or OTX008 + IR relative to those treated with the vehicle control. ***$p_{\text{OTX008 vs. IR + OTX008}} < 0.0001$, ***$p_{\text{IR vs. IR + OTX008}} < 0.0001$; One-way ANOVA followed by Tukey's test for multiple comparisons, n = 6.

Fig. 7. Galectin1 interacts with HOXA5 endogenously in EGFRvIII-expressing BTSCs.

bioRxiv preprint doi: https://doi.org/10.1101/2021.04.14.439704; this version posted April 14, 2021. The copyright holder for this preprint (which was not certified by peer review) is the author/funder. All rights reserved. No reuse allowed without permission.

(**a**) *LGALS1*-differentially genes from RNA-seq analysis were subjected to enrichment analysis of transcription factor (TF) binding motifs using oPOSSUM-3 software. High-scoring or over-represented TF binding site profiles were computed as having z-scores above the mean + 2 x standard deviation (red dotted line). (**b**) Volcano plot representing the HOXA5 targets genes among the *LGALS1*-differentially-regulated genes is shown. *LGALS1*-differentially regulated genes that possess HOXA5 binding sites (HOXA5 targets) are reported as blue dots, *LGALS1*-differentially-regulated genes (DEGs) that do not possess HOXA5 binding sites are reported as red dots and the non-differentially regulated genes (Non DEGs) are represented as black dots. Black lines show RT-qPCR validated cell cycle related genes. (**c**) Relative positions of HOXA5 peaks, obtained from ChIP-seq analysis in human carcinoma cells, to the adjacent TSS of *LGALS1*-differentially regulated genes from RNA-seq analysis are shown. The x-axis indicates the distance between peak centers and the TSS of adjacent *LGALS1*-differentially regulated genes. The y-axis denotes the expression ratios (log2) of the *LGALS1*-differentially regulated gene. Circle size indicates HOXA5 peak height, and color denotes the conservation score of HOXA5 peaks. (**d**) BTSCs were analyzed by immunoblotting using the antibodies indicated on the blots. Wild type EGFR and EGFRvIII bands are marked with * and **, respectively. (**e**) Correlation of HOXA5 expression with galectin1 expression was obtained by running Pearson analyses on the densitometric values of protein expression normalized to tubulin. (**f-g**) BTSCs were electroporated with siCTL or siRNA against *HOXA5* (si*HOXA5*). mRNA levels of the *LGALS1*-downregulated genes that possess HOXA5 motifs were evaluated by RT-qPCR. BTSC73 (**f**): ***$p = 0.0001$ for each pairwise comparison; BTSC147 (**g**): ***$p = 0.0001$ for each pairwise comparison except: **$p_{E2F7} = 0.0014$, **$p_{NDC80} = 0.0099$; One-way ANOVA followed by Dunnett's test, n = 3. Data are presented as the mean ± SEM. (**h**) Representative phase-contrast images of BTSC73 electroporated with si*HOXA5* or siCTL in the absence and presence of 4 Gy are shown. Images were taken following 7 days of plating. Scale bar = 100 µm. (**i**) ELDA was performed following 4 Gy of IR in si*HOXA5* vs. siCTL. (**j**-**m**) Whole cell lysates from BTSC73 (**j**), BTSC147 (**k**) BTSC68 (**l**) and BTSC172 (**m**) were subjected to immunoprecipitation using an antibody against HOXA5 or rabbit IgG control, followed by immunoblotting with galectin1 and HOXA5 antibodies. The Western blots represent a minimum of three replicates from different passage numbers for each BTSC. (**n**-**q**) Proximity ligation assay (PLA) of galectin1 and HOXA5 were performed in BTSC147 (**n**), BTSC68 (**o**), BTSC172

bioRxiv preprint doi: https://doi.org/10.1101/2021.04.14.439704; this version posted April 14, 2021. The copyright holder for this preprint (which was not certified by peer review) is the author/funder. All rights reserved. No reuse allowed without permission.

(**p**) and BTSC73 (**q**). Primary antibodies were omitted for the controls. PLA was performed in *LGALS1* CRISPR in (**q**) as an additional control. Nuclei were stained with DAPI. Images were obtained with a 63X objectives on a laser scanning confocal microscope (ZEISS LSM 800). Scale bar = 10 μm. Representative images of three independent experiments are shown. (**r**) *LGALS1* CRISPR and CTL BTSC73 were subjected to ChIP using an antibody to HOXA5 or IgG control followed by RT-qPCR for four *LGALS1*-downregulated genes that possess HOXA5 binding motifs. HBB locus was used as a negative control. ***p_{ACSS3} (HOXA5 IP in CTL vs. IgG IP in CTL) = 0.0007, **p_{ACSS3} (HOXA5 IP in *LGALS1* CRISPR vs. HOXA5 IP in CTL) = 0.0036, ***$p_{ARIDA5B}$ (HOXA5 IP in CTL vs. IgG IP in CTL) < 0.0001, ***$p_{ARIDA5B}$ (HOXA5 IP in *LGALS1* CRISPR vs. IgG IP in CTL) = 0.0003, **$p_{ARIDA5B}$ (HOXA5 IP in *LGALS1* CRISPR vs. HOXA5 IP in CTL) = 0.0019, ***p_{DSCAM} (HOXA5 IP in CTL vs. IgG IP in CTL) < 0.0001, **p_{DSCAM} (HOXA5 IP in CTL vs. IgG IP in CTL) = 0.0021, **p_{DSCAM} (HOXA5 IP in *LGALS1* CRISPR vs. HOXA5 IP in CTL) = 0.0026, ***p_{KCNK2} (HOXA5 IP in CTL vs. IgG IP in CTL) = 0.0002, *p_{KCNK2} (HOXA5 IP in CTL vs. IgG IP in CTL) = 0.0173, **p_{KCNK2} (HOXA5 IP in *LGALS1* CRISPR vs. HOXA5 IP in CTL) = 0.0028; Unpaired two-tailed *t*-test, n = 3. Data are presented as the mean ± SEM. (**s**) Kaplan-Meier survival plot describing the association between *LGALS1* and *HOXA5* expression and the survival of glioblastoma patients treated with or without radiotherapy. $p_{\text{High } HOXA5/\text{High } LGALS1, \text{ radiotherapy vs. High } HOXA5/\text{High } LGALS1, \text{ non-radiotherapy}}$ = 0.013, $p_{\text{High } HOXA5/\text{High } LGALS1, \text{ radiotherapy vs. Low } HOXA5/\text{Low } LGALS1, \text{ radiotherapy}}$ = 0.007, $p_{\text{Low } HOXA5/\text{Low } LGALS1, \text{ radiotherapy vs. Low } HOXA5/\text{Low } LGALS1, \text{ non-radiotherapy}}$ = 0.022, $p_{\text{Low } HOXA5/\text{Low } LGALS1, \text{ radiotherapy vs. High } HOXA5/\text{High } LGALS1, \text{ non-radiotherapy}}$ = 0.003. (**t**) Kaplan-Meier survival plot describing the association between *LGALS1* and *HOXA5* expression and the progression-free survival of glioblastoma patients treated with or without radiotherapy. $p_{\text{High } HOXA5/\text{High } LGALS1, \text{ radiotherapy vs. Low } HOXA5/\text{Low } LGALS1, \text{ radiotherapy}}$ = 0.070, $p_{\text{Low } HOXA5/\text{Low } LGALS1, \text{ radiotherapy vs. High } HOXA5/\text{High } LGALS1, \text{ non-radiotherapy}}$ = 0.079. Patient survival and gene expression (microarray G4502A Agilent, level 3, n = 489) data were retrieved from TCGA.

Figure 1

bioRxiv preprint doi: https://doi.org/10.1101/2021.04.14.439704; this version posted April 14, 2021. The copyright holder for this preprint (which was not certified by peer review) is the author/funder. All rights reserved. No reuse allowed without permission.

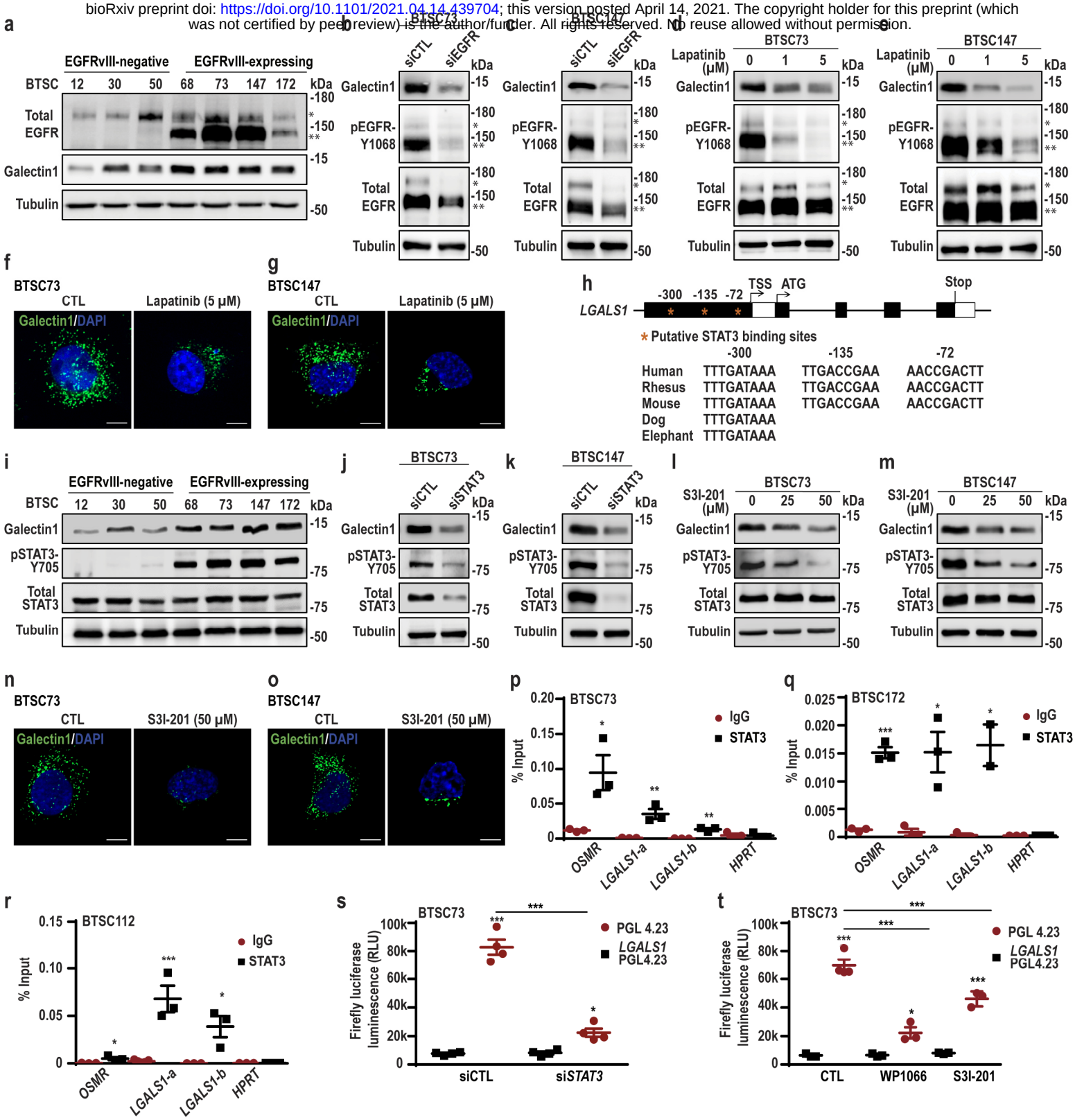

Figure 2

bioRxiv preprint doi: https://doi.org/10.1101/2021.04.14.439704; this version posted April 14, 2021. The copyright holder for this preprint (which was not certified by peer review) is the author/funder. All rights reserved. No reuse allowed without permission.

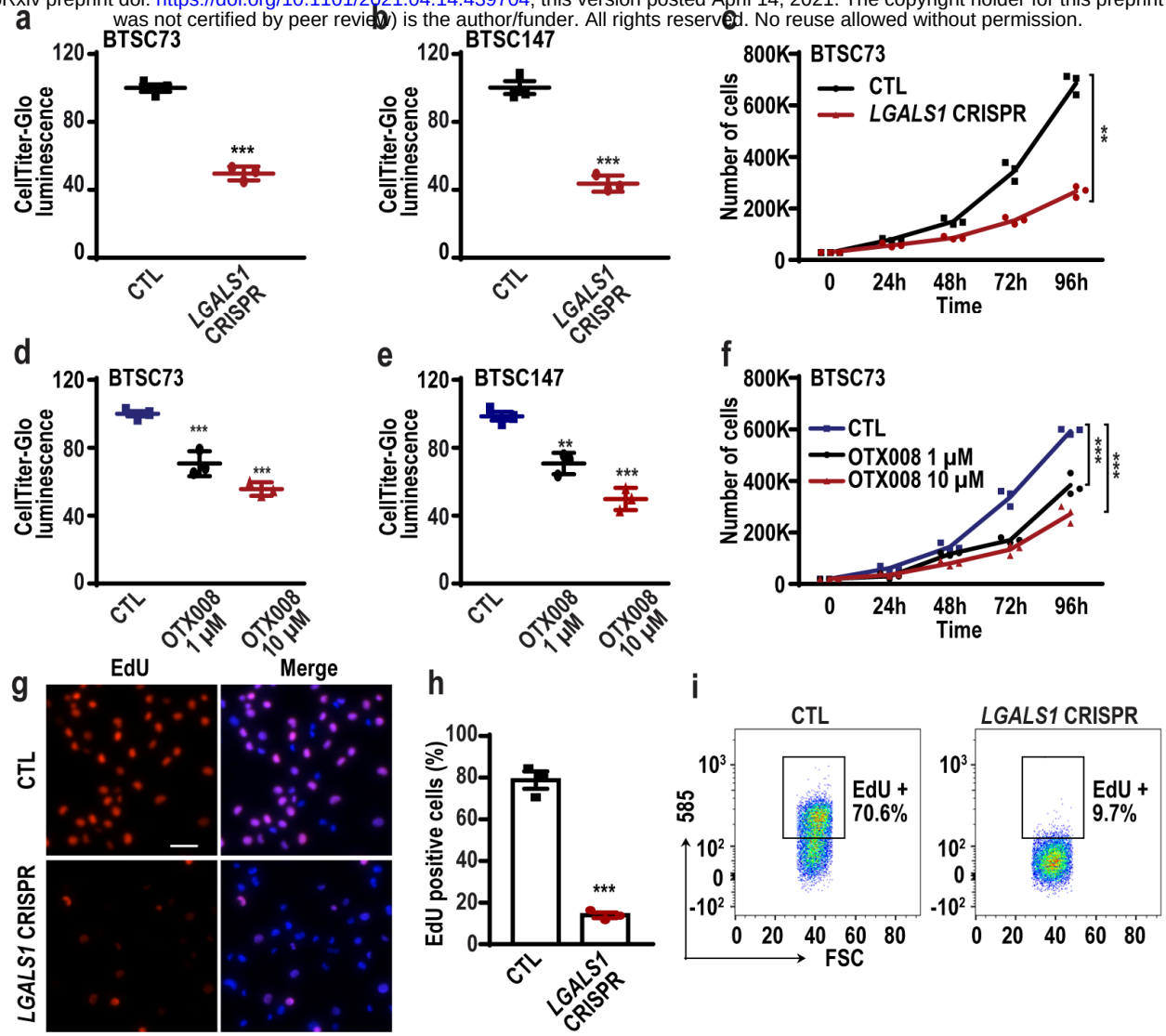

Figure 3

bioRxiv preprint doi: https://doi.org/10.1101/2021.04.14.439704; this version posted April 14, 2021. The copyright holder for this preprint (which was not certified by peer review) is the author/funder. All rights reserved. No reuse allowed without permission.

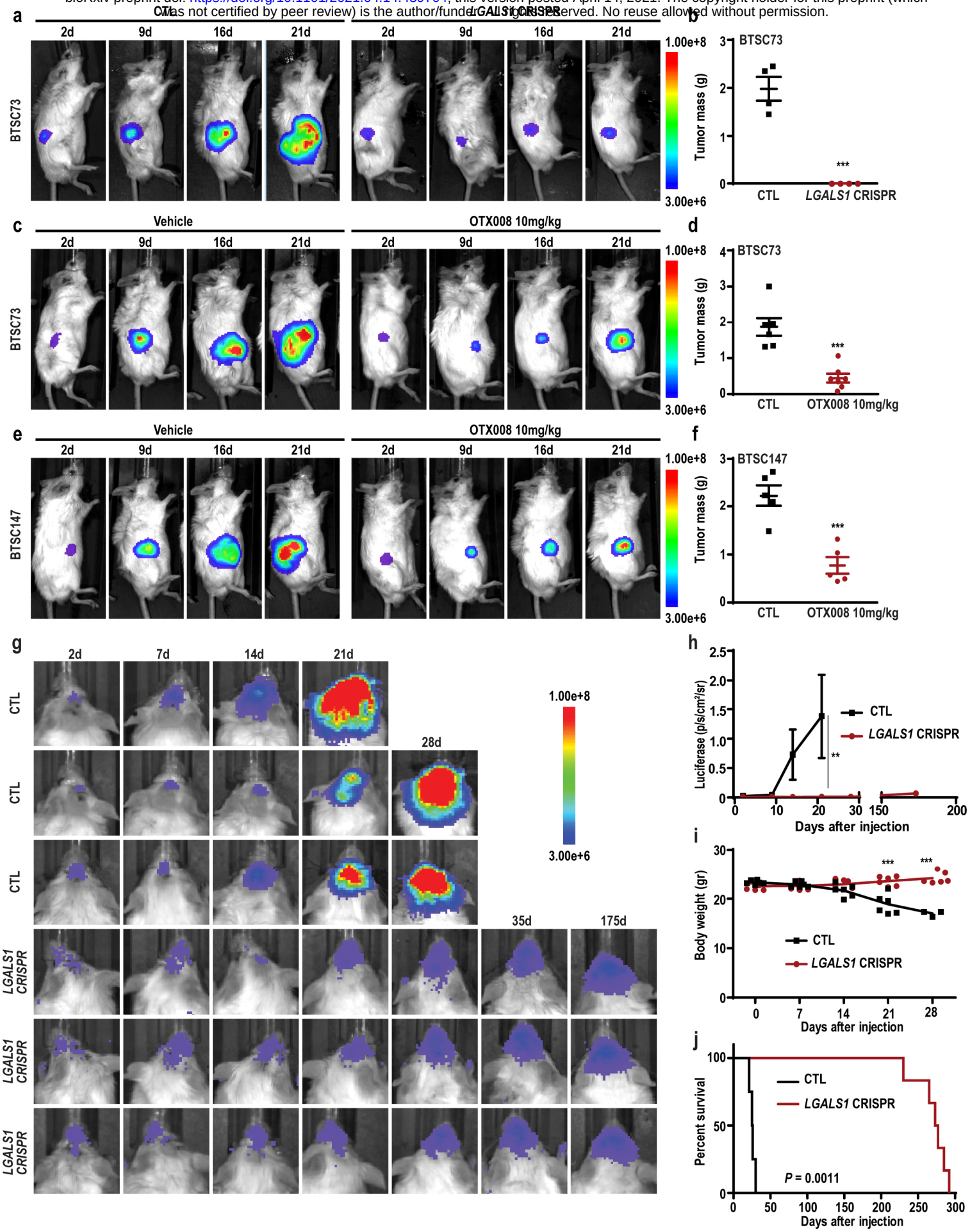

Figure 4

bioRxiv preprint doi: https://doi.org/10.1101/2021.04.14.439704; this version posted April 14, 2021. The copyright holder for this preprint (which was not certified by peer review) is the author/funder. All rights reserved. No reuse allowed without permission.

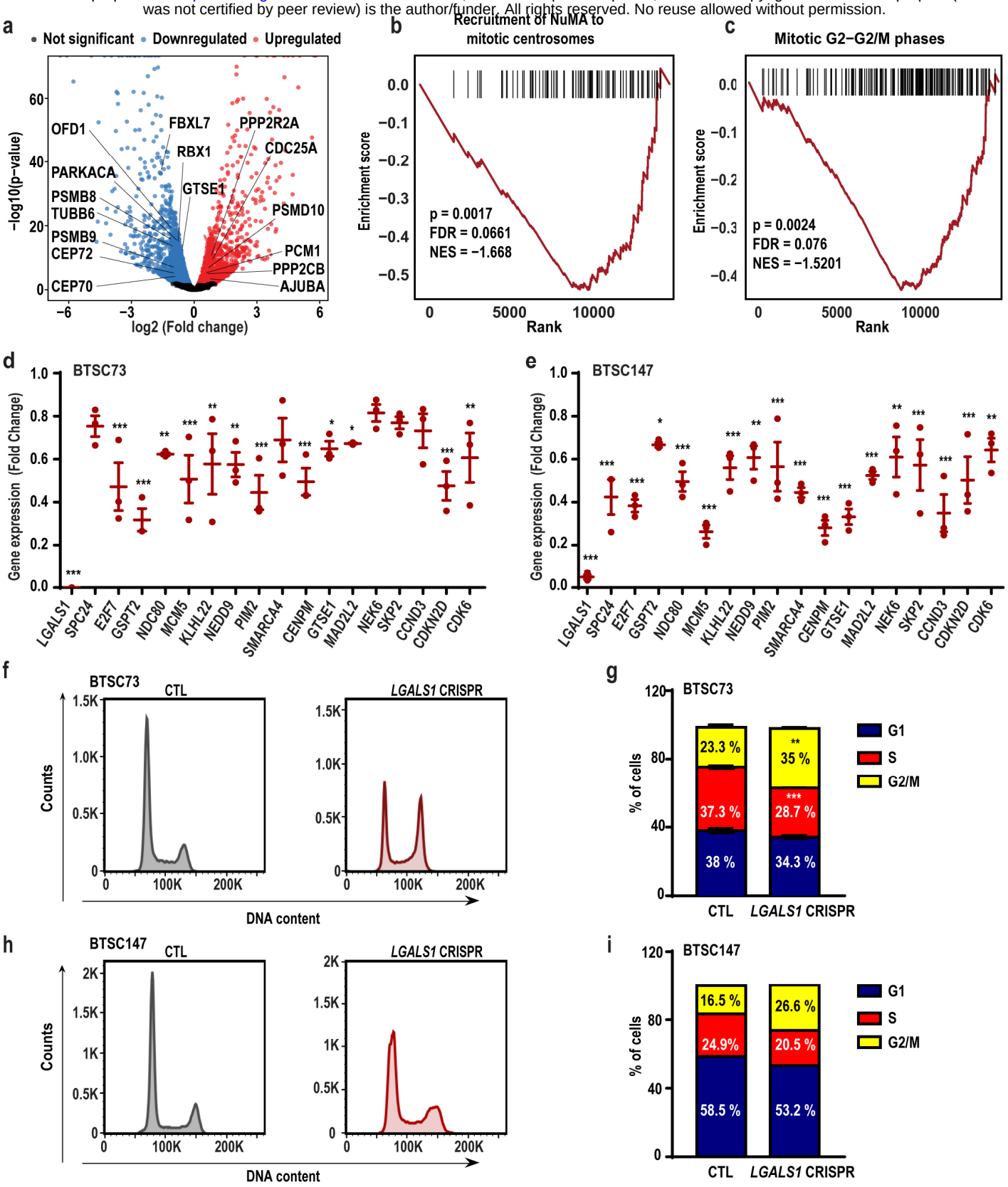

Figure 5

bioRxiv preprint doi: https://doi.org/10.1101/2021.04.14.439704; this version posted April 14, 2021. The copyright holder for this preprint (which was not certified by peer review) is the author/funder. All rights reserved. No reuse allowed without permission.

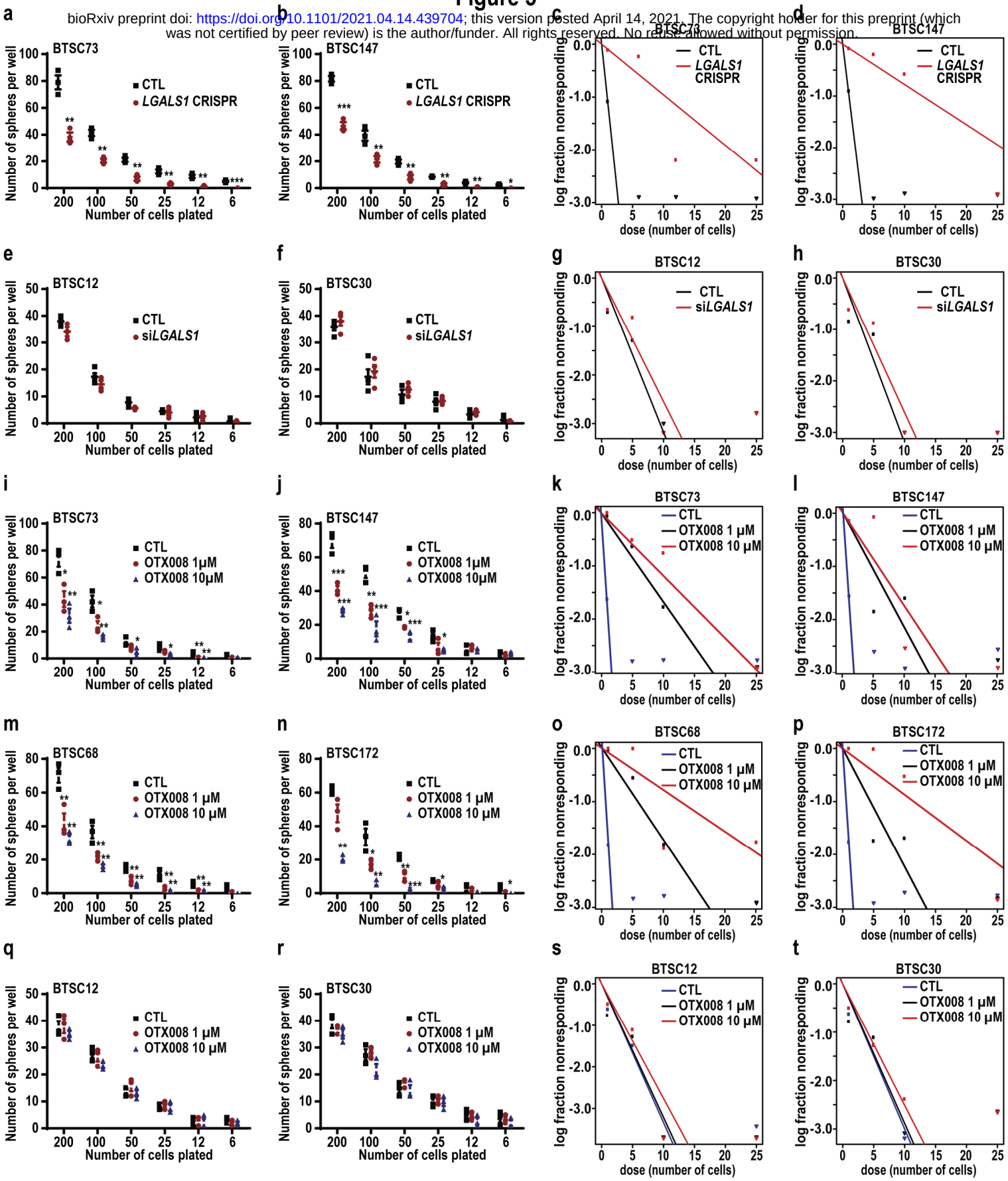

Figure 6

bioRxiv preprint doi: https://doi.org/10.1101/2021.04.14.439704; this version posted April 14, 2021. The copyright holder for this preprint (which was not certified by peer review) is the author/funder. All rights reserved. No reuse allowed without permission.

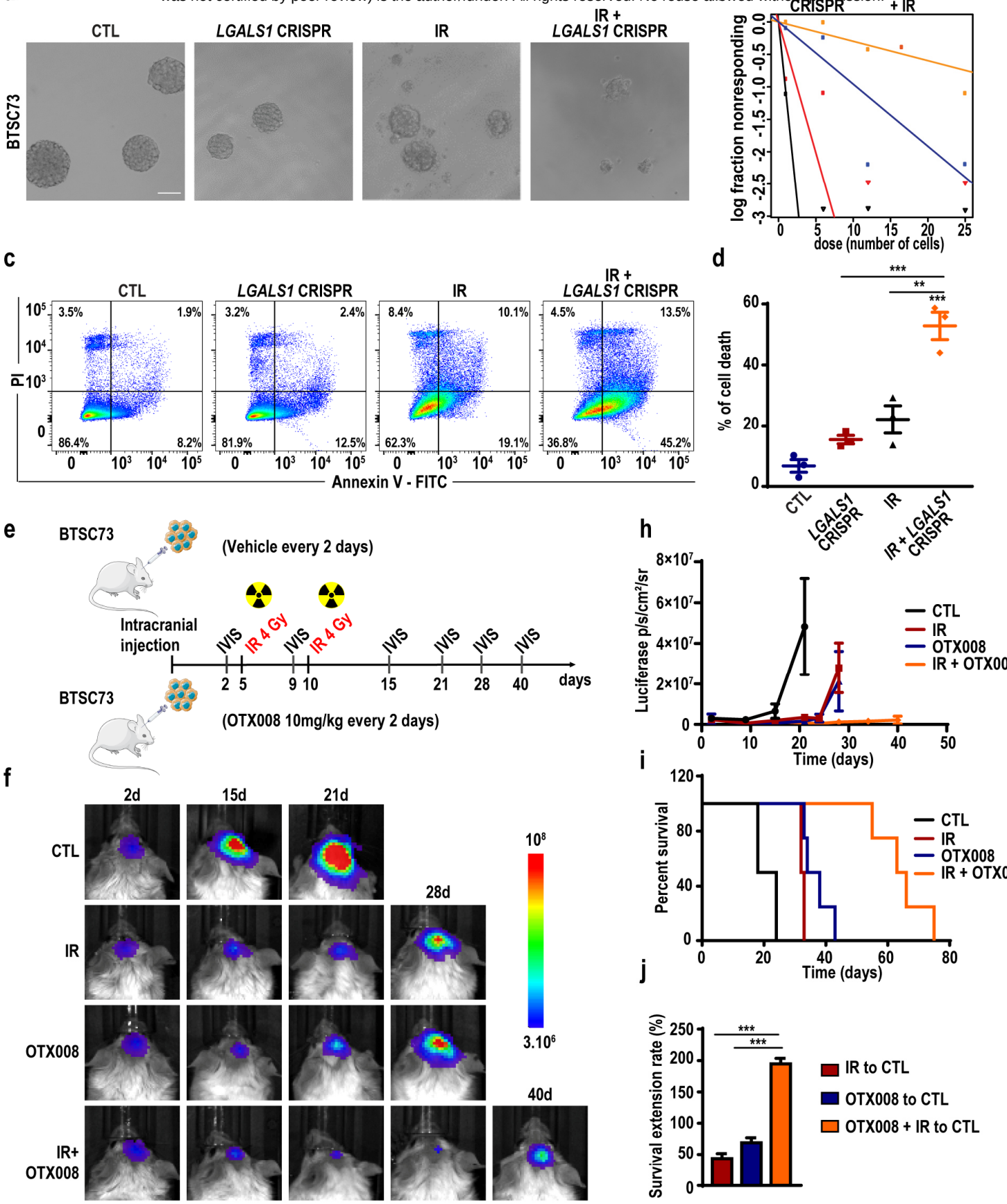

bioRxiv preprint doi: https://doi.org/10.1101/2021.04.14.439704; this version posted April 14, 2021. The copyright holder for this preprint (which was not certified by peer review) is the author/funder. All rights reserved. No reuse allowed without permission.
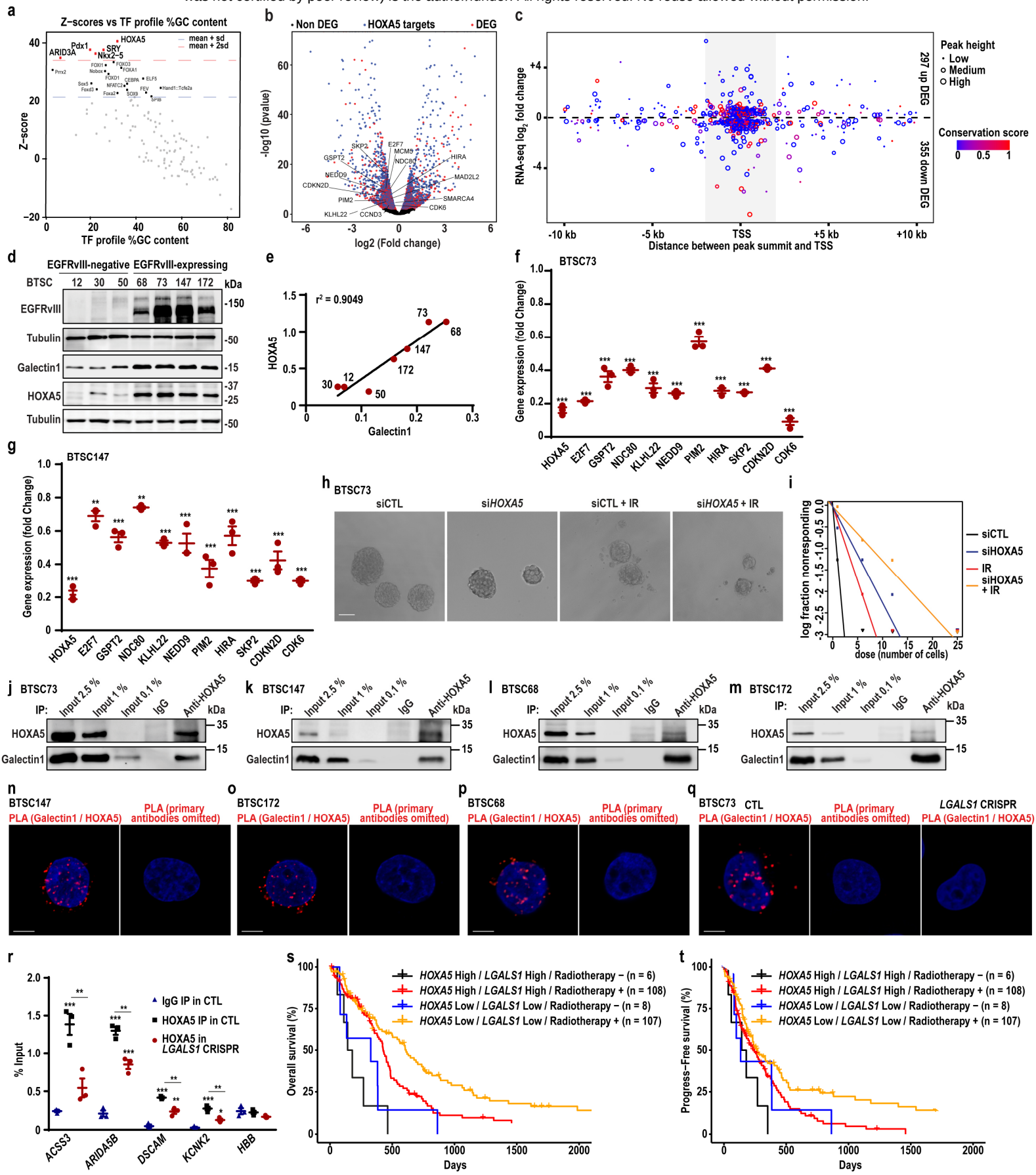
Figure 7